Reply to the editor's comments

We would like to thank the editor for concisely summarizing the concerns of both reviewers and sharing further comments and ideas that have helped us to further improve the manuscript.

Editor comment #1: How would the results and conclusions differ if one box was used that was centered on the maximum EKE?
Reply: This is a good idea. A detailed analysis of a box shifting with the maximum in baroclinic conversion and further comments can be found in our reply to review #2.

Editor comment #2: Both reviewers note that it isn't clear that changes in the baroclinic conversion on cyclone days is that much greater than on non-cyclone days, and I agree. As per reviewer 1's request, some quantification of this statement is required. It seems that the reduction in baroclinic conversion that is not associated with a surface level cyclone is as important to the change in EKE (and perhaps in the midwinter minimum in the maximum EKE) as is the change in vertical structure of cyclones with a surface signature.
Reply: Yes, this is correct, the relative changes are similar. A quantification is given in the revised manuscript and also in the reply to review #1. Absolute values of baroclinic conversion are larger during cyclone days, but the relative change in the conversion on non-cyclone days from November to January is quite similar to that of cyclone days. Note, the definition of non-cyclone days allows that the target region is covered by up to 25% by a surface cyclone. We do agree that baroclinic conversion associated with upper level eddies that are shallow (not extending through the depth of the troposphere) is also suppressed.

Editor comment #3: Reviewer 1 is concerned that the analysis only addresses the changes in EKE in the far western Pacific, and that no evidence is presented for the changes in the central and eastern Pacific.
Reply: We fully agree. We now provide clear statements in the abstract and conclusions. The eastern Pacific requires further investigation. We also adapted the title of our study. For more details see the reply to reviewer #1.

Editor comment #4: A separate question I have (related to a point raised by Reviewer 2) concerns the use of a monthly mean of stability S in the calculation of baroclinic conversion. There is a lot of low frequency variability associated with the stationary wave coming off east Asia: how would the results differ if a low passed version of S was used –the same filter used to estimate theta_bar in this calculation?
Reply: During the preparation of the data for Schemm and Rivière (2019), which uses the same data set, we tested different ways to compute S and the results only marginally differed. We thus decided to stick to the traditional way of defining S based on a vertical reference temperature profile of the monthly mean as in Cai and Mak (1990) or Orlanski and Katzefy (1991).

Reply to the reviewer's comments

Anonymous Referee #1

We would like to thank both reviewers for carefully evaluating our manuscript and for providing comments that helped us to further improve our study.

Reviewer: The paper exclusively focuses on the western Pacific, and does a good job of accounting for midwinter suppression in that region. However, that region covers less than half of the area in the Pacific basin where suppression is observed to occur, which stretches eastward all the way to N America (Fig 1b). The authors note that their focus region is "located at the entrance of the storm track" (l.126), implying that eddies in that region will subsequently move downstream, so that the eastern part of the storm track will behave similarly to the western part. The implicit message is that a theory for suppression in the western region will also explain suppression in the Pacific storm track as a whole. But is this really true? After all, cyclones have a marked bias to poleward propagation, and it's not obvious they will follow the purely zonal propagation required by this implicit statement.
I think that leaving the reader guessing about this point risks being misleading, and requires clarification. For example, the authors could use the cyclone track data to show that cyclones passing through the northwestern "suppressed" box do indeed go on to feed the eastern part of the stormtrack where suppression is observed. Alternatively, they could omit further analysis, but provide a clear statement (in the abstract and conclusions) that mechanisms responsible for suppression in the east require further analysis.

Authors: This is an excellent point. We focus on the part of the storm track over the western North Pacific where baroclinicity is largest in midwinter. The cyclone tracks analyzed in our study have their lysis on average poleward of 50° N in the central Pacific. The Pacific storm track is known to "restart" over the central Pacific. Hoskins and Hodges (2002; p. 1060) noted "*that very few synoptic systems can be tracked along the length of the Pacific storm track. Indeed, most of the systems generated over eastern Asia do not even reach the mid-Pacific. It is the systems that are generated in the central-east Pacific that occlude on the northwest coast of North America.*" A finding, which was later confirmed by Wernli and Schwierz (2006; Figs. 9c and 9d). Indeed, a large fraction of the cyclogenesis over the eastern Pacific is secondary cyclogenesis (Schemm et al. 2018; Fig. 5b). We therefore fully agree with the reviewer that our study, focusing on the western North Pacific, does not address midwinter suppression of the entire Pacific storm track. To potentially explain the suppression over the eastern Pacific, it could be rewarding to explore suppression of the downstream development (Simmons and Hoskins 1979, Orlanski and Chang 1993), which would be of high scientific merit and should be reserved for a follow-up study.
In the revised manuscript, we adapted the title and we provide a clear statement in the abstract and the conclusions that we focus exclusively on the western North Pacific where climatological mean baroclinicity is highest and that the suppression over the eastern Pacific requires additional analysis.

Minor comments

- l. 46: "Subtropical jet regime": For the reader not deeply versed in the current literature, it would be useful to give a brief explanation of what you exactly mean by this expression (and what other regimes are possible).
  Authors: We added an explanation.

- l. 66: "propagate in tandem poleward": Fig 21 in Hoskins et al 1985 and surrounding text do not actually say anything about preferential poleward propagation, so far as I can see; the poleward propagation mechanisms instead are discussed in later work for example by Gwendal Riviere and Talia Tamarin, and possibly others I'm not familiar with. Some citations to literature on poleward propagation should be inserted here. This is clearly also relevant to my main comment above.
  Authors: Yes, we added more appropriate references. It is long-standing knowledge from case studies (Palmén and Newton 1969), also discussed in idealized experiments (Hoskins and West 1979, Davies et al. 1991) and later from feature-based climatologies (e.g., Hoskins and Hodges 2002) that cyclone tracks are deflected poleward. Important recent studies about the underlying mechanism are by Gilet et al. (2009), Rivière et al. (2012) and Tamarin and Kaspi (2017). In our study, the poleward motion can be inferred from Fig. 3, which shows that less than 20% of all cyclone tracks in the Gulf of Alaska are generated over the Kuroshio.

- l. 110: please state the cutoff frequency used for the high-pass filtering.
  Authors: We added this information. It is 10 days.

- l. 117: The analysis of EKE and baroclinic conversion in this and later sections is all carried out at 500 hPa. This choice needs some justification. Would analysis at other levels, or in the vertical average, give the same qualitative results and conclusions?
  Authors: The level is a pragmatic choice. The midwinter increases with altitude (Schemm and Schneider 2018), but baroclinic conversion is typically largest in the lower troposphere. At the 500 hPa level, baroclinic conversion is still large and the midwinter suppression is a well-marked feature in the conversion rates. Qualitatively, we expect the same results for vertical averages or integrals. For example, the study by Schemm and Schneider (2018) was based on vertically integrated conversion rates and yielded comparable results. The location of our target regions is also not affected by the choice of the level and all results related to the surface cycle tracks are thus largely independent of the vertical level.

- Fig 1: It would be useful to show a plot of cyclone track densities overlayed on EKE to appreciate their relationship (this could be done directly in Fig 1, or separately in supplementary material to avoid clutter).
  Authors: We show cyclogenesis frequencies and considered adding the surface cyclone frequencies to Fig. 1 and Fig. 3., but the cyclone frequency peaks poleward of the EKE maximum and provide no new insight into the nature of the suppression. A figure showing EKE and surface cyclone frequencies overlayed is Fig. 1 in Schemm and Schneider (2018). Following the reviewer's suggestion, we show the mean position of the tracks (Fig. R2 in reply document to Reviewer #2) and we will add it to the final version our study.

- l. 163, Table 1: please specify what exact genesis regions are used to define Kamchatka, Kuroshio and East China Sea cyclones.
  Authors: We added this information to the table.

- l. 216 and elsewhere: I recommend sticking to the expression "feature tracking" or "cyclone tracking", rather than the vague and potentially misleading "quasi-Lagrangian". Many studies (including some by these authors) combine true Lagrangian analysis with feature tracking, in which case the inappropriateness of "quasi-Lagrangian" becomes obvious. Better for the community to have a single word for a single concept.
  Authors: We fully agree and removed “quasi-Lagrangian” from the manuscript.

- l. 245: Surface cyclones do not necessarily correspond only to deep (troposphere filling) eddies; they could also be shallow, diabatically maintained eddies. Some rewording may be needed here.
  Authors: Correct, we adapted the sentence accordingly.

- l. 265: Some quantification would be useful here: what fraction do cyclone days/non-cyclone days cumulatively contribute to mean baroclinic conversion, and to the suppression in January?
  Authors: On cyclone days, the conversion reduces from 17 x 10^4 J/kg/s in November to 6.4 x 10^4 J/kg/s in January and on non-cyclone days from 13 to 3.4 x 10^4 J/kg/s in the same period. In both categories, we find that the suppression is approximately 10 x 10^4 J/kg/s and the number of days in both categories is about 50%. In the revised paper, we highlight this more prominently. We also include the exact numbers in the corresponding section. We also emphasize that a non-cyclone day might still be affected by a cyclone, which propagates in close proximity or along the edge of the target region. But it is now correctly mentioned that baroclinic conversion on non-cyclone days is equally affected by the suppression and the relative reduction is similar.

- lines 292 and 301: Seems to me, by eye from Fig 6, that mean baroclinicity is reduced from Nov to Jan by about the same amount for both Kuroshio and Kamchatka cyclones. It’s possible I’m misunderstanding here, in which case please clarify this point.
  Authors: This is correct, mean baroclinicity reduces by the same amount for both cyclone categories from November to January. We added a new panel to Fig. 6, which shows the conversion efficiency. It is not only the reduction in mean baroclinicity that matters, but Kuroshio and Kamchatka cyclones also become less efficient in converting the mean baroclinicity into eddy total energy. The reduction in baroclinicity and conversion efficiency contribute both to the reduction in baroclinic conversion. For example, the mean baroclinicity over the northern target region is similar for Kuroshio and Kamchatka cyclones, however Kamchatka cyclones have lower conversion rates due to an overall lower conversion efficiency. But it is correct, the relative change from November to January in the mean baroclinicity and conversion efficiency is for both the same. We clarified our reasoning in this section.

Literature:

Davies, H. C., Schär, C., & Wernli, H. (1991). The palette of fronts and cyclones within a baroclinic wave development. Journal of the atmospheric sciences, 48(14), 1666-1689.

Gilet, J. B., Plu, M., & Rivière, G. (2009). Nonlinear baroclinic dynamics of surface cyclones crossing a zonal jet. Journal of the atmospheric sciences, 66(10), 3021-3041.

Hoskins, B. J., & Hodges, K. I. (2002). New perspectives on the Northern Hemisphere winter storm tracks. Journal of the Atmospheric Sciences, 59(6), 1041-1061.

Orlanski, I., & Chang, E. K. (1993). Ageostrophic geopotential fluxes in downstream and upstream development of baroclinic waves. Journal of the atmospheric sciences, 50(2), 212-225.

Palmén, E. H., & Newton, C. W. (1969). Atmospheric circulation systems: their structure and physical interpretation (Vol. 13). Academic press.

Rivière, G., Arbogast, P., Lapeyre, G., & Maynard, K. (2012). A potential vorticity perspective on the motion of a mid-latitude winter storm. Geophysical research letters, 39(12).

Schemm, S., Sprenger, M., & Wernli, H. (2018). When during their life cycle are extratropical cyclones attended by fronts?. Bulletin of the American Meteorological Society, 99(1), 149-165.

Schemm, S., & Schneider, T. (2018). Eddy lifetime, number, and diffusivity and the suppression of eddy kinetic energy in midwinter. Journal of Climate, 31(14), 5649-5665.

Simmons, A. J., & Hoskins, B. J. (1979). The downstream and upstream development of unstable baroclinic waves. Journal of the Atmospheric Sciences, 36(7), 1239-1254.

Tamarin, T., & Kaspi, Y. (2017). Mechanisms controlling the downstream poleward deflection of midlatitude storm tracks. Journal of the Atmospheric Sciences, 74(2), 553-572.

Wernli, H., & Schwierz, C. (2006). Surface cyclones in the ERA-40 dataset (1958–2001). Part I: Novel identification method and global climatology. Journal of the atmospheric sciences, 63(10), 2486-2507.

Reply to the reviewer's comments

Anonymous Referee #2

We would like to thank both reviewers for carefully evaluating our manuscript and for providing comments that helped us to further improve our study.

Reviewer: After reading the paper and thinking of the results I am wondering why the authors did not define a single EKE target region, which moves from month to month with the EKE maximum, and performed the analysis this way, i.e. examining the storms which reach each month's region, separated to the different cyclogenesis regions. This would reduce confusion between a reduction of EKE due to a shifting relative to the averaging domain and a real overall reduction of the total storm energy. The main hesitation I have with the approach taken here is the fact that the two regions span around 15- and 10-degrees latitude-order of 1000-1500 km, which is on the order of typical cyclone radii. Thus, I am guessing a cyclone will feel parts of both regions as it evolves and propagates along its track. The interpretation of a latitudinal shift in terms of a dipole is less intuitive on a single storm scale. It sounds intuitive reading the paper since the authors discuss tracks that pass through each region but that in some sense gives a wrong picture. I am not saying the approach is wrong but the authors should somehow justify it, at the very least by a discussion of spatial scales, why they choose to divide the domain this way, and how the results relate to the physical picture of single cyclones. Best will be of course to compare the analysis for single regions which shift with the EKE maximum.

Authors: We very much thank the reviewer for these thoughtful comments and we appreciate the suggestion of choosing a target box that shifts with the EKE maximum.

During January and March, the EKE maximum at the 500 hPa level is located over the mid-Pacific, but in November over the eastern Pacific (black contours in Fig. R1). The corresponding cyclone tracks are generated in very different environments (cyclogenesis frequencies are shown in Fig. R1). Hoskins and Hodges (2002; p. 1060) noted *"that very few synoptic systems can be tracked along the length of the Pacific storm track. Indeed, most of the systems generated over eastern Asia do not even reach the mid-Pacific. It is the systems that are generated in the central-east Pacific that occlude on the northwest coast of North America."* We argue that comparing cyclone tracks generated in such different environments is potentially confusing. Instead, in agreement with Reviewer #1, we propose to focus on the western North Pacific where the maximum in baroclinic conversion occurs throughout the winter. Climatologically, mean baroclinicity is highest over the western Pacific and it increases from November to January (green contours in Fig. R2). Similar to the suppression of EKE, there is, however, a reduction of the baroclinic conversion during this time period (black contours in Fig. R2), which is "unexpected" given the increase in baroclinicity. We therefore propose a modification of the suggestion by the referee and choose a target region that shifts with the maximum in baroclinic conversion over the western Pacific.

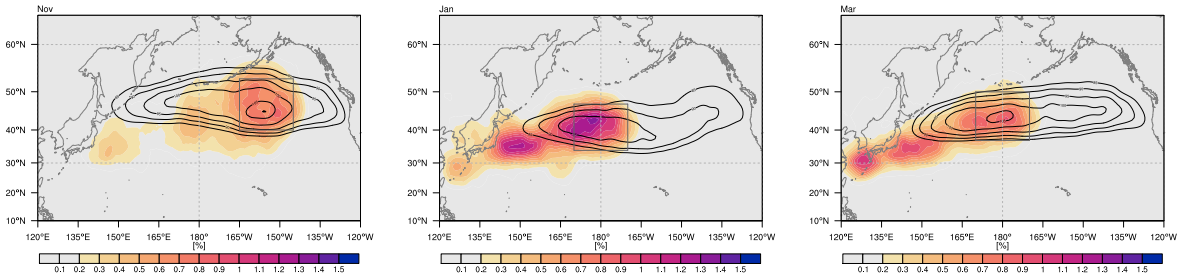

Figure R1: Cyclogenesis frequency (color shading; %) for surface cyclone tracks that propagate through a target region (shown as a gray box) that shifts with the EKE maximum for (left) November, (mid) January and (right) March. EKE at 500 hPa is shown by black contours.

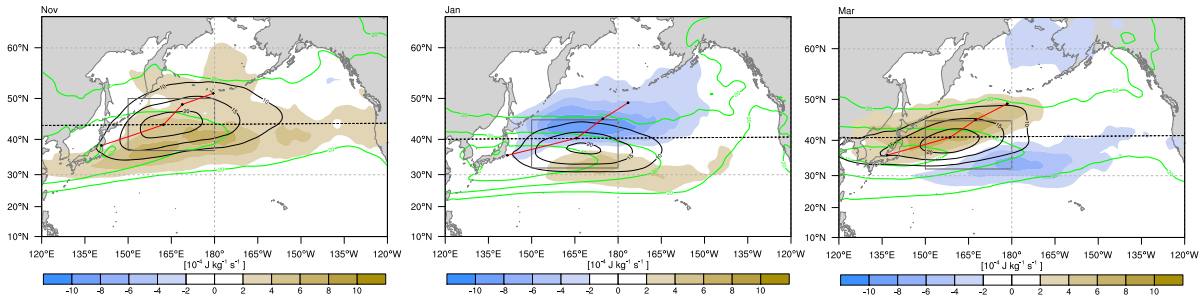

Figure R2: Baroclinic conversion at 500 hPa (black contours; 10^4 J kg-1 s-1) and change relative to the previous month (shading). Gray boxes denote a target region that shifts with the maximum in baroclinic conversion. Also shown is the mean position of cyclone tracks that enter the target region from upstream (red line), with black dots marking the mean position of cyclogenesis, maximum deepening (6-hourly SLP change), maximum intensity (minimum SLP) and cyclolysis.

A target region that shifts with the maximum in baroclinic conversion is shown in Fig. R2. Also shown as a red line is the mean position of the cyclone tracks that propagate into this region from upstream, excluding tracks with genesis in the box (Fig. R1). The first black dot indicates the mean cyclogenesis location, the second the mean location of maximum deepening (6-hourly SLP change), the third the location of maximum intensity (minimum SLP), and the fourth indicates the mean cyclolysis location. During November and March, the location of maximum deepening (second dot) coincides with the maximum in monthly mean baroclinic conversion (black contours). During January, it is slightly north of it. We now repeat the statistical analysis of these tracks. To this end, we split all tracks in time steps before and after the tracks cross the latitude of the monthly mean maximum deepening (shown as the dashed line in Fig. R2) and we next analyze baroclinic conversion averaged in a 1000 km radius at every time step before and afterwards (similar as in the main manuscript).

The corresponding box-and-whisker plot of baroclinic conversion (Fig. R3) shows that baroclinic conversion is highest in January but only before the maximum deepening is reached (this is in agreement with highest baroclinicity in January at latitudes equatorward of the latitude of maximum conversion). Once the tracks have passed the location of maximum deepening, the baroclinic conversion is reduced relative to the time steps before maximum deepening (compare black to gray box-and-whiskers in every month in

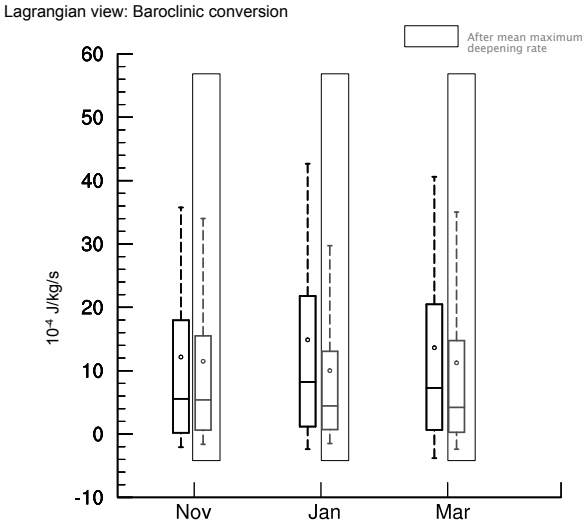

Figure R3: Box-and-whisker diagram for baroclinic conversion at 500 hPa (104 J kg-1 s-1) averaged within a radius of 1000 km around the surface cyclone centers of surface cyclone tracks that enter the target region shown in Fig. 2 from upstream for time steps south of (black) and north of (gray) the maximum deepening (6-h SLP change).

Fig. R3) but baroclinic conversion is now also suppressed in January relative to November in March (compare gray box-and-whiskers between the different months). This is in agreement with the red mean cyclone track in Fig. R2, which on its way poleward propagates out of the contours of largest monthly mean baroclinic conversion in January (black contours in Fig. R2) but in November and Marc. Overall, the results nicely complement our results presented in our manuscript in Fig. 6, where we split the tracks in time steps inside and outside of a "northern target region". We will add the above new results as a new section to the revised manuscript and we thank the reviewer for suggesting a shifting target box.

Reviewer: Also, it is not clear at the moment if the main contribution of the paper is in elucidating the changes in the eddies which contribute to the midwinter suppression and the dependence on the cyclogenesis region, or if it provides a more fundamental understanding by further by also explaining the changes in the eddies. For the latter, the authors need to tighten the discussion of how the results fit in with existing theory.

Authors: The main goal of our study is to describe how the life cycle of cyclones generated in the different genesis region, which all affect the region of suppression in the western North Pacific, changes during midwinter.

Reviewer: The main underlying theory - that equatorward shifting of the jet results in a weakening of the storms due to their meridional tilt, inherently looks at the entire storm and how its meridional shift varies with height - the division into poleward and equatorward parts in this argument does not necessarily make sense.

Authors: We are undecided to which argument in our manuscript the reviewer is referring to. We separate the cyclone tracks into sections equatorward and poleward of a critical latitude (above in Fig. R2 the latitude of maximum baroclinic conversion) but unrelated to the vertical tilt.

Reviewer: The argument that the baroclinicity shifts equatorwards into the Kuroshio cyclogenesis region during midwinter, suggests at first that the storms should grow more efficiently during mid-winter, but the overall argument made is that they grow less efficiently. I think the answer to this is given in the summarizing argument, on lines 338-345, but I am not sure I fully understand it- do the authors mean to say that the larger meridional tilt seen in Schemm and Riviere is in a sense an artifact of the time averaging over the cyclone life cycle, and since the cyclone moves poleward quicker, while undergoing faster growth and decay as it shifts poleward, the time averaged structure has a stronger tilt? Thus, the overall growth over the full cyclone life cycle is what becomes less efficient? This in essence sounds similar to the original arguments by Nakamura (1992), that storms grow faster but also move quicker, but instead of the stronger zonal wind advecting the storms out of the baroclinicity region, the storms move poleward and they undergo the full nonlinear life cycle of growth and decay.

Authors: We added the baroclinic conversion efficiency to our analysis. It is shown in the revised Fig. 6 of the manuscript and shown below as Fig. R4 of this document. Similar as before, we split the Kuroshio tracks into time steps outside and inside of the northern target region. As suggested by the reviewer, the cyclones are more efficient in January compared with November and March as long as they are equatorward of the target region, but once they propagated poleward and outside the baroclinic zone they quickly become less efficient. This is in agreement with what is shown in brown and blue shading Fig. R4 in Schemm and Rivière (2019). We hope that this clarifies our reasoning: First the cyclones are more efficient and baroclinic conversion rates are large, but further poleward their efficiency is reduced. We do

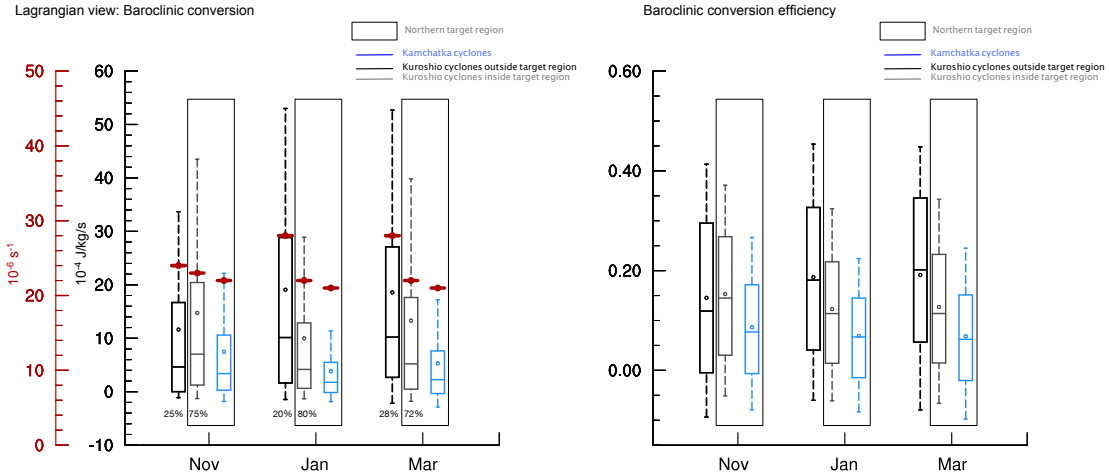

Figure R4: (revised version of Fig. 6 in the manuscript): Box-and-whisker diagram for (left) baroclinic conversion at 500 hPa (10-4 J kg-1s-1) averaged within a radius of 1000 km around the surface cyclone centers of Kuroshio and East China Sea cyclones, before (black) and after (gray) entering the northern target region, and for Kamchatka cyclones (blue). Additionally, shown are the mean background baroclinicity along the tracks (red horizontal lines) and the percentage of time steps before and after entering the target region. (right) Similar as in the left panel but for the baroclinic conversion efficiency (unitless).

not estimate the propagation speed nor do we perform any time averaging along the tracks, but we do agree that in essence the argumentation is similar to Nakamura (1992) that storms move quicker out of the baroclinicity region, but they also become less efficient on their way poleward. We add this link to the original 1992 paper to the corresponding section.

Reviewer: Schemm and Riviere discuss Nakamura and Sampe's argument that the growth is less efficient on a strong and subtropical jet due to a stronger meridional tilt which the storms assume if their surface cyclogenesis remains at the same latitude. They point out that the meridional-vertical tilt implied by Nakamura's argument (equatorwards with height) is opposite to the tilt they find (poleward with height). They mention that the meridional tilt would be different for different seeding latitudes (I assume this is part of the motivation for this paper). I think the authors should more explicitly tie the current results to this argument, and specifically does the change found in Kamchatka cyclone life cycles fit with the argument of Nakamura and Sampe?

Authors: We try to tie our work better to the previous literature using Fig. R4 to which we added the baroclinic conversion efficiency. The figure shows that the cyclones become less efficient when propagating poleward. The main motivation of this paper is the life cycle perspective: How does the conversion and the efficiency change during the life cycle and which cyclones contribute to the reduction in the baroclinic conversion? In Schemm and Rivière (2019) we speculate that the argument of Nakamuara and Sampe applies to the southern seeding branch. According to Chang (2005), the southern seeding branch is associated with East China Sea cyclones (though the upper level waves do not necessarily trigger East China Sea cyclones) and can also sometimes trigger Kuroshio cyclones (though they are mostly triggered by the northern seeding branch). To connect the individual cyclone tracks to one of the two seeding branches would be beyond the scope of this study.

Reviewer: The main results for the Kamchatka cyclones (lines 334-337): "The fraction of explosively deepening cyclones first reduces from November to January but then remains at similar levels until March. Highest values in baroclinic conversion are found during midwinter, but these occur at lower latitudes, south of the northern target region, and they are sustained for a reduced number of time steps. In terms of minimum sea level pressure, Kuroshio cyclones are most intense in January." The finding of a reduction in explosive cyclogenesis but more intense cyclones during January is confusing. Also- is it obvious why the growth in mid-winter is sustained for less time?

Authors: We tried to clarify this point. The fraction of "bomb" cyclones reduces (deepening larger than 24 hPa in 24 hours normalized to 60° N as in Sanders and Gyakum 1980) from November to January, but the largest 6-hourly baroclinic conversion rates are still observed during January. They are maintained for a shorter time period, which matters most for the overall deepening. We do not know if this is obvious, but the life time of cyclones reduces in midwinter and the number of time steps with high growth rates is lowered.

Reviewer: Figure 2: What is counted as propagation through a region- that the cyclone track which follows the cyclone center (a single pixel of minimum pressure?) pass through it, or a part of the cyclone (the region of 1's corresponding to the detection scheme) passes through it? Similarly- the cyclogenesis is counted as the whole cyclone or its center?
Authors: For the selection of the tracks we use the minimum SLP as the center of the cyclone and the cyclone center must be at least once within the target region. We added this information to the manuscript. For the cyclogenesis, we compute a radius of 500 km around the genesis location to define a "genesis region". In this way, all genesis events are treated equally.

Reviewer: Figure 3: I am not sure I understand what is shown here - the caption says "relative contributions...to the total surface cyclone frequency in the northern target region", which implies a very wide cyclogenesis region to the west and north of the target region, which is not what I expect, and I am not sure how this fits with figure 2..? The plots look more like the contribution to total cyclone frequency from those cyclones originating in the target area. But then the percentage is out of the total cyclones contributing to the target region, but not including cyclones which miss the target region? so the sum of the right and left columns add to 100% in the target region but not outside of it? An explicit explanation of how the fields in figure 3 relate to those in figure 2 might help clear things.
Authors: The plot needs a better explanation. The plots are the contribution to the total cyclone frequencies propagating through the target area not originating from the target area. Additionally, we separate those that enter the target area from the south from all others, which essentially separated Kuroshio and East China Sea cyclones from Kamchatka cyclones. In the target region it adds up to 100% but not outside.

Reviewer: Do you have any idea why the number of Kamchatka cyclones decreases and the number of East china sea cyclones increase as the season progresses?
Authors: We do not have an explanation for the increase in East China Sea cyclones. For Kamchatka cyclones is seems to be the reduction in the mean baroclinicity and eventually also a reduction in the upper-level seeding, but this hypothesis would require further testing.

Reviewer: Section 2: Methodology - using a monthly mean static stability alongside low and high pass filtered quantities - how do you deal with the jumps in static stability in between months? how much does the static stability change from month to month? Do you use the climatology or each year's monthly mean?
Authors: During the preparation for the study of Schemm and Rivière (2019), we tested different filters and averaging windows and did not find a significant difference. For the static stability, the reference temperature profile is in agreement with the traditional literature computed from a climatological monthly mean.

Reviewer: The discussion on page 7 needs some tightening - there is repetition of the results of the previous sections and within the section itself.
Authors: Page 7 is the method section; we would appreciate if the reviewer could point us to the corresponding section that needs some tightening because we are unsure whether the reviewer refers to page 17 or section 7.

Reviewer: line 265- Please state explicitly why you say the non cyclone days contribute *much* more than non cyclone days- they clearly contribute more but its not clear on quick look that its all that much more. Being more quantitative might help.

Authors: In the revised version, we give the exact numbers of the change from cyclone days and non-cyclone days between November and January. We highlight the fact that cyclone days have much higher values in baroclinic conversion, but, as pointed out correctly by both reviewers, the changes are about the same (revised l. 275-280).

Reviewer: line 278- the authors average at a radius of 1000km around the cyclone center. 1000km is roughly the latitudinal length of the southern box, so if the cyclone is at the southern edge of the EKE decrease box, the averaging could include a very large portion of the EKE increase region as well. . . is this problematic and how does this affect the results? see major comment above.

Authors: Yes, this is correct, if the cyclone is near the southern edge of the northern target region it will tap into the southern target region. In Schemm and Rivière (2019) it was shown that when using a radius of 2000 km or an average inside the outermost closed SLP contour used for the tracking, the results are qualitatively still very similar to the 1000 km radius, though smaller (larger) in absolute values, respectively. We believe that the increase/decrease pattern in EKE is partly a result of the changes in baroclinic conversion along the tracks of the analyzed cyclones and when a cyclone affects first the southern box, for some time steps both target regions and further poleward only the northern target region then this is what results in the climatological mean and a transition zone does not seem to be problematic for the interpretation of our results.

The ~~North Pacific~~ Storm-Track Suppression ~~Explained~~ over the Western North Pacific From a Cyclone Life-Cycle Perspective

Sebastian Schemm[1], Heini Wernli[1], and Hanin Binder[1]

[1]Institute for Atmospheric and Climate Science, Universitätstrasse 16, 8092 Zürich, Switzerland

Correspondence: sebastian.schemm@env.ethz.ch

Abstract. Surface cyclones that feed the western part of the North Pacific storm track ~~experiencing~~ and experience a midwinter suppression originate from three regions: the East China Sea (∼30°N), the Kuroshio extension (∼35°N), and downstream of Kamchatka (∼53°N). In midwinter, in terms of cyclone numbers, Kuroshio (45%) and Kamchatka (40%) cyclones dominate in the region where eddy kinetic energy is suppressed, while the relevance of East China Sea cyclones increases from winter (15%) to spring (20%). The equatorward movement of the baroclinicity and the associated upper-level jet toward midwinter influences cyclones from the three genesis regions in different ways. In January, Kamchatka cyclones are less numerous, less intense and their lifetime shortens; broadly consistent with the reduced baroclinicity in which they grow. The opposite is found for East China Sea cyclones, which in winter live longer, are more intense, and experience more frequently explosive deepening. The fraction of explosive East China Sea cyclones is particularly high in January when they benefit from the increased baroclinicity in their environment. Again, a different and more complex behavior is found for Kuroshio cyclones. In midwinter, their number increases, but their lifetime decreases; on average they reach higher intensity in terms of minimum sea level pressure, but the fraction of explosively deepening cyclones reduces and the latitude where maximum growth occurs shifts equatorward. Therefore, the life cycle of Kuroshio cyclones seems to be accelerated in midwinter with a stronger and earlier but also shorter deepening phase followed by an earlier decay. Once they reach the latitude where eddy kinetic energy is suppressed in midwinter, their baroclinic conversion efficiency is strongly reduced. Together, this detailed cyclone life-cycle analysis reveals that the North Pacific storm-track suppression in midwinter is related to fewer and weaker Kamchatka cyclones and to more equatorward intensifying and then more rapidly decaying Kuroshio cyclones. The less numerous cyclone branch from the East China Sea partially opposes the midwinter suppression. The cyclones passing through the suppressed region over the north-western Pacific do not propagate further downstream into the eastern Pacific but have their lysis further poleward and in the mid-Pacific. The eastern Pacific requires further analysis.

1 Introduction

Nakamura (1992) identified the contrasting intraseasonal cycles of the North Atlantic and North Pacific storm tracks in winter. While different measures of storm-track activity over the Atlantic experience a single peak in midwinter, the Pacific storm-track activity has two peaks, one in late autumn and another one in early spring (Nakamura, 1992). Over the North Atlantic, the seasonal cycle of the baroclinic wave amplitude is broadly consistent with the seasonal cycle of mean baroclinicity, but this is

not the case over the North Pacific where the midwinter suppression of the storm-track activity occurs at the time of maximum surface baroclinicity and jet strength. The midwinter suppression affects a large number of eddy measures, such as the eddy heat and momentum fluxes and the eddy kinetic energy, as well as the baroclinic and barotropic conversion rates, whereas measures of the mean background flow, such as the monthly mean jet strength and the Eady growth rate are not affected by the suppression (Schemm and Schneider, 2018). The midwinter suppression is most pronounced in the upper troposphere and almost absent in the lower troposphere. Also, the total number of surface cyclones does not experience a suppression (Schemm and Schneider, 2018). The atypical intraseasonal cycle of baroclinic waves over the North Pacific has triggered considerable research during the last two decades. In the following, we give an overview of the current understanding of the midwinter suppression.

Factors that have been suggested to contribute to the midwinter suppression can be categorized into contributions from barotropic, baroclinic and upstream-seeding processes. Among the barotropic contributions are the increase of the horizontal wind shear near the jet and the deformation acting on baroclinic wave packets in a stronger and more narrow jet stream during midwinter (James, 1987; Nakamura, 1993; Harnik and Chang, 2004; Deng and Mak, 2005). However, in idealized simulations it was shown that such a barotropic governor mechanism is not symmetric in time around the suppression and the increase in the horizontal shear lags the onset of the suppression (Novak et al., 2020). With regard to upstream seeding processes, a reduction in the amplitude and frequency of upper-level eddies propagating from upstream into the North Pacific has been suggested to play a crucial role in the formation of the midwinter suppression (Penny et al., 2010, 2011, 2013), but this is strongly debated because baroclinic growth is decorrelated with the strength of upstream seeding (Chang and Guo, 2011, 2012). Moreover, a reduced midwinter suppression also occurs in simulations with the upstream Asian mountains removed (Park et al., 2010). The increase in the velocity of eddy propagation along the baroclinic zone and a reduced lifetime has also been shown to be insufficient to explain the suppression (Chang, 2001; Nakamura and Sampe, 2002). The reduction in the lifetime also occurs over the North Atlantic, which does not exhibit a suppression in most winters (Schemm and Schneider, 2018).

There is mounting evidence that the shift to a subtropical jet regime in the western North Pacific is essential for the formation of the midwinter suppression. During the shift to a subtropical jet regime, the subtropical thermally-driven jet increases its strength, shift equatorward and extends into the zonal direction. Idealized studies have shown that the transition to a subtropical jet regime is able to reproduce a realistic midwinter suppression and thus ruled out the absolute necessity of zonal asymmetries, such as upstream mountains, for its formation (Yuval et al., 2018; Novak et al., 2020). The importance of a subtropical jet regime for the formation of a storm-track suppression is reinforced by the fact that a mild suppression is also observed over the North Atlantic in years with strong subtropical jets (Penny et al., 2013; Afargan and Kaspi, 2017). Chang (2001) and Nakamura and Sampe (2002) already hinted at the potential key role of the subtropical jet and its meridional displacement relative to the low-level zone of highest baroclinicity, but the exact mechanism that reduces baroclinic growth remained unclear. Such a mechanism was suggested by Schemm and Rivière (2019), who showed that in the subtropical jet regime the ability of eddies to extract eddy energy from the mean baroclinicity is reduced because of a reduction in the baroclinic conversion efficiency. Eddies from the northern seeding branch (Chang, 2005) propagate more equatorward and towards the subtropical jet in midwinter and during this equatorward propagation they acquire a stronger than usual poleward tilt with height, which

reduces the eddy efficiency because of a weaker alignment between the mean baroclinicity and the eddy heat flux (Schemm and Rivière, 2019). Schemm and Rivière (2019) quantified baroclinic conversion for all upper-level eddies and surface cyclones in the western North Pacific. However, as shown in section 4 of this study, the surface cyclone tracks in this sector of the Pacific emerge from three different regions: (i) downstream of Kamchatka, (ii) over the Kuroshio extension, and (iii) over the East China Sea. So far, it is unclear if the suppression affects the cyclones from these genesis regions in a similar way.

In this study, we investigate midwinter changes in surface cyclone life cycles over the western North Pacific according to their genesis region. Surface cyclones are an important subcategory of the wide distribution of flow features collectively termed "eddies". Upper-level cyclonic eddies, some of them shallow, correspond to troughs. Once a trough interacts with a surface eddy, they mutually amplify (Hoskins et al., 1985, Fig. 21) and propagate in tandem poleward ~~(Hoskins et al., 1985, Fig. 21)~~ (Gilet et al., 2009; Rivière et al., 2012; Oruba et al., 2013). The combined system develops into a mature low-pressure system corresponding to a deep cyclonic eddy. With surface cyclone tracks we thus identify particularly strong cyclonic eddies that play an essential role for the overall storm track climatology. Over the North Pacific, we expect to find different life-cycle characteristics in midwinter compared to November and March, because in midwinter the cyclones typically form on the poleward flank of a strong subtropical jet, whereas in November and March they usually develop on the equatorward flank of a more poleward located jet. Schemm and Schneider (2018) have already shown that for the entire North Pacific the lifetime of surface cyclones decreases. Here we study in detail all surface cyclones that affect the region of the midwinter suppression in the western North Pacific between October and April and quantify their frequency, lifetime, intensity, baroclinic conversion rates, and other characteristics according to their genesis region. This approach will serve to address the following questions:

- What is the relative contribution of different genesis regions to the surface cyclone frequency in the region affected by the midwinter suppression?
- Are there any differences in the character of the surface cyclones of different origin between midwinter and the shoulder months? For example, how does their number, lifetime and time to maximum intensity vary during the cold season?
- Is the suppression of the baroclinic conversion during midwinter equally strong for cyclones of different origin?

To answer these questions, we use an object-based surface cyclone tracking algorithm and evaluate baroclinic conversion rates obtained from bandpass-filtered data along individual cyclone tracks. With this approach, we combine two complementary perspectives on storm track dynamics.

Our study is organized as follows. In section 2 we introduce the used data and methods. In section 3 we describe the midwinter evolution of eddy kinetic energy (EKE) over the North Pacific and define specific target regions characterized by an increase and decrease in EKE during winter, respectively. The surface cyclone tracks and the genesis regions of cyclones that propagate through the target regions are presented in section 4. section 5 presents a detailed analysis of changes in different life cycle characteristics, including maximum deepening rates. Baroclinic conversion along cyclone tracks of different origin are studied in section 6. We conclude our study in section 7.

2 Data and Methods

The analysis period is October to April 1979–2018. All diagnostics rely on 6-hourly ERA-Interim data that are interpolated to a 1° grid. ERA-Interim is publicly available for download via ECMWFs archive at https://apps.ecmwf.int/datasets/.

2.1 Surface-cyclone tracks and surface cyclogenesis

For the identification and tracking of surface cyclones, we make use of the algorithm introduced by Wernli and Schwierz (2006) and refined by Sprenger et al. (2017). The detection of surface cyclones is based on a contour search in the mean sea level pressure (SLP) field at intervals of 0.5 hPa. To obtain a cyclone mask at each time step, all grid points inside the outermost closed contour, which must not exceed 7500 km in length, are labelled with 1, all others with 0. The obtained binary cyclone fields are used to compute cyclone frequencies. Cyclone centers are defined as the grid point with minimum SLP inside the outermost closed contour. The cyclone centers are tracked using 6-hourly cyclone center positions, and a track is accepted if it exists for a period of at least one day. The first time step along each track is defined as the genesis time step and the SLP minimum defines the genesis location. The algorithm contributed to the cyclone identification and tracking intercomparison project of Neu et al. (2013).

2.2 Baroclinicity and baroclinic conversion

The background baroclinicity and the corresponding baroclinic conversion are defined based on tendency equations for eddy kinetic and available potential energy (Lorenz, 1955; Orlanski and Katzfey, 1991; Chang, 2001). A detailed derivation of both tendency equations using 10-day high-pass-filtered input data is given in Schemm and Rivière (2019). The baroclinic conversion to eddy energy, the sum of eddy kinetic and eddy available potential energy, is the scalar product between the eddy heat flux $\frac{1}{\sqrt{S}}\theta' \mathbf{v}'$ and the background baroclinicity $-\frac{\nabla\overline{\theta}}{\sqrt{S}}$,

$$B_{conv} = -\frac{1}{S}\theta' \mathbf{v}' \cdot \nabla\overline{\theta} \tag{1}$$

where $\mathbf{v}'$ denotes the high-pass-filtered horizontal wind, $\overline{\theta}$ the low-pass-filtered potential temperature, and S the static stability in pressure coordinates $S = -h^{-1}\frac{\partial\theta_R}{\partial p}$. The reference potential temperature θ_R is computed from monthly mean data and h denotes the scale height. Background baroclinicity is defined as the horizontal gradient of the low-pass-filtered potential temperature divided by the static stability, $\boldsymbol{B} = -\frac{\nabla\overline{\theta}}{\sqrt{S}}$. The background baroclinicity is closely related to the Eady growth rate (Lindzen and Farrell, 1980). The ~~data used in this study is similar to that used in Schemm and Rivière (2019). For the low-pass filter a 10-day cut-off period is used as in Rivière et al. (2018) and Schemm and Rivière (2019).~~ scalar product that defines the baroclinic conversion can further be decomposed into contributions from the mean baroclinicity and the baroclinic conversion efficiency – for details see Schemm and Rivière (2019). We base our analysis on the conversion rates at the 500 hPa level. This is a pragmatic choice, because the suppression extends in amplitude with altitude, while baroclinic conversion is largest in the lower troposphere (Schemm and Schneider, 2018). At the 500 hPa level, the suppression of baroclinic conversion is a well-marked feature.

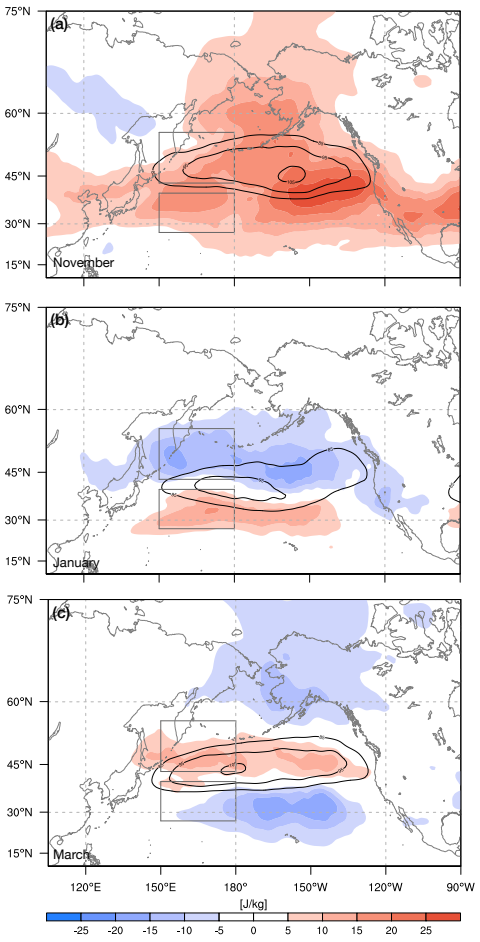

Figure 1. Mean EKE at the 500 hPa level (black contours at 85, 95, and 105 J kg^{-1}) and corresponding change relative to the corresponding previous month (color shading) for (a) November, (b) January and (c) March. Additionally shown are two target regions (gray boxes) that are used for the detailed diagnostics of surface cyclone tracks throughout this study.

3 EKE of the North Pacific storm track in midwinter

This section recapitulates the seasonal cycle and transition of the North Pacific storm track as seen in EKE at 500 hPa. In November, EKE increases, relative to October, across the entire North Pacific (red shading in Fig. 1a), with the maximum increase over the eastern North Pacific near 150°W. In January, EKE reduces compared to December in an elongated band across the Pacific north of ∼43° (blue shading in Fig. 1b). Equatorward of this latitude, however, EKE increases (red shading in Fig. 1b). This dipole pattern in EKE tendency results from the equatorward shift of the North Pacific jet during midwinter. Absolute values of EKE (black contours in Fig. 1b) are reduced compared to those in November, which is due to the stronger

Table 1. (First column) Total number of surface cyclones in the northern target region and number of cyclones per day in parenthesis (1980–2018). (Second column) Fraction and number (in parenthesis) of Kamchatka, (third column) Kuroshio and (fourth column) East China Sea cyclones. The northern target region is shown in Fig. 1. Kuroshio and East China Sea cyclones have their genesis south of 45°N and east of 135°E and west of 135°E, respectively.

	Cyclones in target region	Kamchatka	Kuroshio	East China Sea
November	507 [0.43]	45 % [229]	41 % [207]	14 % [71]
January	516 [0.43]	40 % [206]	46 % [236]	14 % [74]
March	527 [0.44]	39 % [208]	39 % [204]	22 % [115]

EKE reduction poleward of ∼43°N compared to the simultaneous increase equatorward [see Fig. 1 in Schemm and Schneider (2018) for a more detailed discussion of month-to-month EKE variations]. From February to March, EKE increases again in a meridionally confined band between ∼40° and 50°N and decreases equatorward of ∼40°. Based on theses patterns of intraseasonal changes in EKE, we select in the following surface cyclones that propagate through one of the regions with a midwinter (December to January) EKE decline or increase, respectively. The two target regions are indicated as gray boxes in Fig. 1 and are located at the entrance of the storm track (EKE maximum). One of our aims is to assess if and how the EKE tendency dipole seen in Fig. 1b is linked to characteristics of the surface cyclone tracks. We focus in particular on cyclones that propagate through the northern target region, which exhibits a decline in EKE during midwinter and is therefore essential for understanding the midwinter suppression phenomenon.

4 Surface-cyclone view on the North Pacific storm track in midwinter

4.1 Surface cyclogenesis

Consideration is first given to cyclogenesis associated with surface cyclone tracks that propagate through the northern target region, i.e., the region where EKE decreases during midwinter (Fig. 1b). To this end, we extract all tracks for which the cyclone core is insight the target region for at least one time step. In November, these surface cyclones originate from two preferred regions (Fig. 2a). The first region is located over the Kuroshio extension (near 35°N) and the second region downstream of the Kamchatka Peninsula (near 53°N). This pattern and the number of events are fairly similar in January (Fig. 2c). In March (Fig. 2e), a third cyclogenesis region emerges southwest of Japan at over the East China Sea (near 30°N), while the other two cyclogenesis regions retain fairly similar frequencies. For cyclones propagating through the target region of the midwinter suppression, there is no signal of a suppression in the genesis and therefore number of these cyclones (Tab. 1).

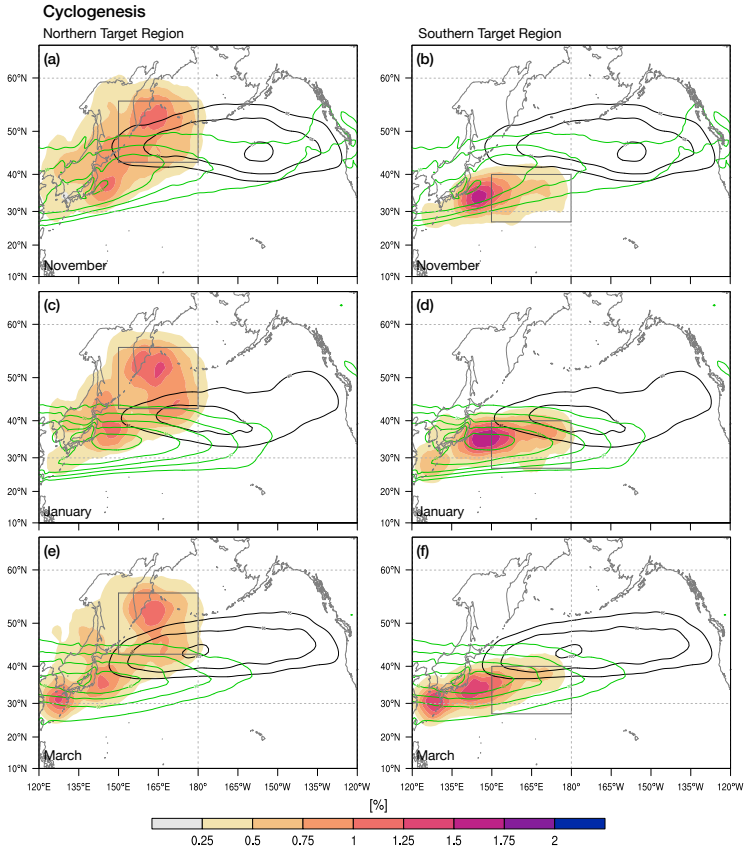

Figure 2. Cyclogenesis frequency (color shading; %) for surface cyclone tracks that propagate through the northern (left column) and southern (right column) target regions (shown as a gray box) for (a,b) November, (c,d) January and (e,f) March. Additionally shown are EKE (black contours; 85, 95, and 105 J kg^{-1}) and baroclinicity (green contours; 25 to 45 by steps of 5×10^{-6}s^{-1}) at the 500-hPa level

The southern target region, i.e., the region where EKE increases during midwinter (Fig. 1b), is fed exclusively by surface cyclones with genesis over the Kuroshio extension during November (Fig. 2b). In January, a second but weaker cyclogenesis region emerges southwest of Japan over the East China Sea. In March (Fig. 2f), the two genesis regions exhibit similar cyclogenesis frequencies and contribute equally to the cyclone tracks in the southern target region. Notably, also for this region there is no midwinter suppression in the cyclone frequency. This result is in agreement with the findings of Schemm and Schneider (2018) that the suppression is connected to a reduction in the cyclone intensities rather than their frequencies.

Surface cyclones over the North Pacific are known to be triggered by two upper-level seeding branches: a northern branch over Siberia and a southern branch along the subtropical jet across southern Asia (Chang, 2005). We briefly report about the upper-level seeding associated with the three preferred regions of surface cyclogenesis (Fig. 2) by means of lagged 300 hPa geopotential anomalies. We find that Kamchatka and Kuroshio cyclogenesis is triggered by waves entering the North Pacific

from the northern seeding branch over Siberia (Supplementary Figure S1), which, in January, have a more equatorward propagation direction, in agreement with Schemm and Rivière (2019). After surface cyclogenesis, the upper-level wave packet retains its overall more zonal orientation (Supplementary Figure S1). Cyclogenesis over the East China Sea is associated with the southern seeding branch and an upper-level trough downstream of the genesis location (not shown). This behavior was already recognized by Chang (2005), who noted that "cyclogenesis for these cases is probably not triggered by the [upper-level] wave packet" (Chang, 2005, p.1998). The genesis of these cyclones seems to be connected to a bottom-up development, as is the case for diabatic Rossby waves (e.g., Boettcher and Wernli, 2013).

4.2 Relative surface cyclone frequencies

In the previous section, we showed that surface cyclogenesis downstream of Kamchatka, over the Kuroshio extension and, in late winter, over the East China Sea, contribute to the surface cyclone tracks in the northern target region, where EKE exhibits a midwinter suppression. ~~The latter two enter the target region from the south, while Kamchatka cyclone have their genesis inside the target region.~~ To study the relative importance of the tracks generate in the different genesis regions for the ~~suppression~~total cyclone frequency in the target region and elsewhere, we group the cyclone tracks ~~that affect the northern target region~~ into two categories. The first contains tracks with genesis over the Kuroshio or the East China Sea ~~,~~ and which enter the target region from the south. The second category contains tracks with genesis near Kamchatka ~~. The~~ that propagate through the target region. Next, we compute cyclone frequency fields for the two categories ~~are then divided~~ at every grid point and divide them by the total cyclone frequency field obtained from all ~~tracks that propagate through the northern target region. These~~ cyclone tracks. The obtained relative contributions are shown for November, January and March in Fig. 3. During all months, Kamchatka cyclones contribute up to 40–50% along the poleward side of the target region and only 10–20% along the equatorward side. The relative contribution of cyclone tracks entering the target region from the south is 80–90% along the equatorward side and 50–60% along the poleward side of the target region. ~~This~~ By definition, they add up to 100% in the target region. The relative contributions also indicate the tendency of the selected cyclone tracks to propagate poleward. For example, less than 20% of the cyclone tracks propagated from the Kuroshio region across the Pacific and into the Gulf of Alaska. Fig. 3 further corroborates that the midwinter suppression is related to a change in the characteristics of these cyclones and not in their frequencies. Also, we cannot focus on Kuroshio or Kamchatka because the contribution of both to the total cyclone frequency in the target region is non-negligible. In the following, we study statistics of cyclone characteristics for the different genesis regions in greater detail.

5 Detailed characteristics of surface cyclone life cycle

In the previous section, we showed that the northwestern Pacific surface storm track is fed by three preferred cyclogenesis regions: (i) East China Sea, (ii) Kuroshio and (iii) Kamchatka; and neither of the three exhibits a midwinter suppression in terms of cyclogenesis frequency (Fig. 2). Next, we investigate several life cycle characteristics. As in the previous sections, our focus is on the northern target region (gray box in Fig. 1), where EKE decreases during midwinter.

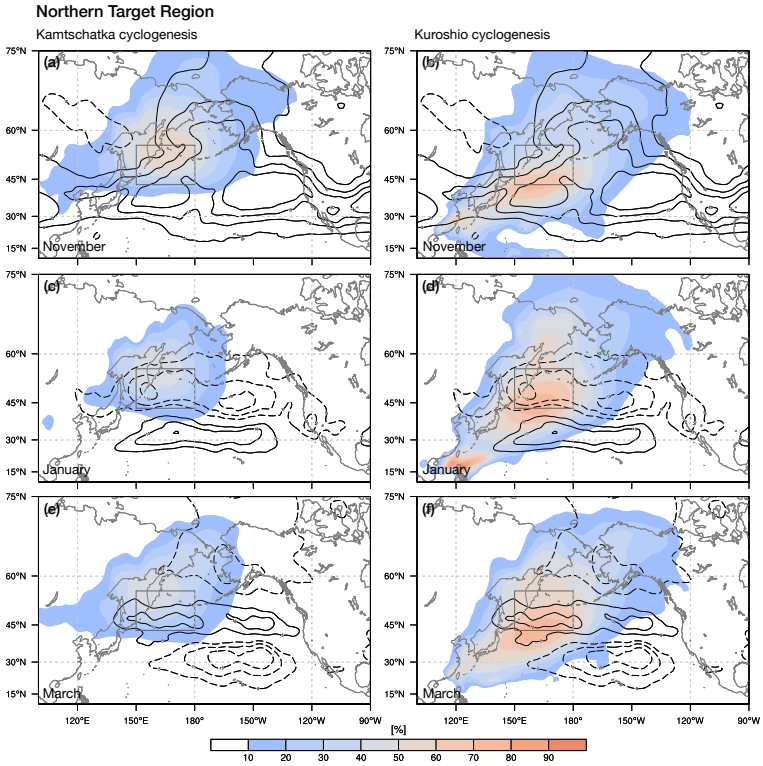

Figure 3. Relative contributions (color shading; %) of (a, c and e) Kamchatka cyclones and (b, d and f) Kuroshio combined with East China Sea cyclones to the total surface cyclone frequency in the northern target region (gray box). The contours show the change in EKE relative to the corresponding previous month (solid lines are for positive values, and dashed lines for negative values; -20 to 20 J kg^{-1} by steps of 5 J kg^{-1}).

As mentioned in the previous section, the total number of cyclones and the number of cyclones per day in the northern target region (first column in Tab. 1) does not exhibit a midwinter suppression and appears to be relatively constant from November to March. However, the detailed picture for the three different genesis regions is more complex. The fraction and number of Kamtschatka cyclones is highest in November and decreases to March. Kuroshio cyclones exhibit a midwinter maximum, which is in agreement with the highest background baroclincity occurring during this time period. The fraction of East China Sea cyclones reveals the exact opposite behavior of Kamtschatka cyclones. Their number and fraction increases from November to March, which is in agreement with the cyclogenesis frequency climatology (Fig. 2e). However, their relevance for the total cyclone climatology is far below that of Kamchatka and Kuroshio cyclones.

The lifetime from genesis to lysis of Kamchatka and Kuroshio cyclones is shortest in January and larger in November and March (Tab. 2). This is what one might expect from the strong midwinter jet and the fact that also over the North Atlantic lowest cyclone lifetimes are observed during midwinter (Schemm and Schneider, 2018). However, it could also result from the

Table 2. Lifetime (hours) of surface cyclones passing through the northern target region according to their genesis regions.

	Kamchatka	Kuroshio	East China Sea
November	77	98	117
January	62	86	132
March	70	91	172

Table 3. Time to maximum deepening since genesis (hours) of cyclones passing through the northern target region according to their genesis regions.

	Kamchatka	Kuroshio	East China Sea
November	35	29	43
January	26	21	39
March	31	23	42

fact that these poleward propagating cyclones leave the more equatorward located baroclinic zone earlier. Finally, the lifetime of East China Sea cyclones increases from November to March.

The time to maximum deepening since cyclogenesis is shortest during midwinter, independent of the cyclogenesis region (Tab. 3). Hereby, maximum deepening is measured in Bergeron, which is the 24-hour change in sea level pressure along a cyclone track normalized to 60°N (Sanders and Gyakum, 1980). Because the cyclogenesis regions exhibit almost no variations in terms of their exact location (Fig. 2), the reduced time to maximum deepening for Kuroshio and East China Sea cyclones could result from the more equatorward location of the zone of highest baroclinicity. These poleward propagating systems eventually leave the baroclinic zone earlier in midwinter, which explains the reduced lifetime and the shorter time to maximum deepening. For Kuroshio and East China Sea cyclones, the mean latitude where maximum deepening occurs is therefore also shifted by around 2° equatorward in January compared to November (not shown), which is in agreement with the earlier deepening.

With regard to the minimum sea level pressure as a measure of the storm intensity, Kamchatka cyclones become less intense from November to March (Tab. 4). East China Sea cyclones are most intense during midwinter, but they contribute only by 22 % to the total cyclone number (Tab. 1). Kuroshio cyclones are also most intense in January, but the change in minimum

Table 4. Minimum sea level pressure of surface cyclones passing through the northern target region according to genesis regions and, in parenthesis, the fraction of cyclones satisfying the criterion for "bomb cyclogenesis" (deepening larger than 24 hPa within 24 hours normalized to 60°N.)

	Kamchatka	Kuroshio	East China Sea
November	979.4 [21 %]	975.8 [49 %]	975.7 [63 %]
January	982.9 [7 %]	973.6 [42 %]	967.2 [76 %]
March	987.3 [7 %]	979.0 [43 %]	971.4 [65 %]

SLP between November and January is small. The equatorward movement of the baroclinic zone in midwinter seems to be beneficial for the intensification of East China Sea cyclones in January. Kamchatka cyclones, however, become less intense, a result that can, at least qualitatively, be expected from the equatorward retreat of the baroclinic zone. For Kuroshio cyclones the situation is complex. While there is a weak reduction in the minimum SLP from November to January, the fraction of life cycles that satisfy the Sanders and Gyakum (1980) criterion for explosive deepening, known as "bomb cyclogenesis"[1], is reduced in midwinter. In contrast, for the East China Sea cyclones the bomb fraction peaks in January, which is in agreement with the increase in the background baroclinicity. Kuroshio cyclones thus appear to deepen rapidly in a short time period (Tab. 3), in agreement with the midwinter peak in baroclinicity, but after reaching their strongest intensity they also decay rapidly, as indicated by the shortest life time during midwinter (Tab. 2). This suggests that for Kuroshio cyclones the peak in baroclinic conversion occurs earlier during their life cycle and short deepening is also more intense, but thereafter they move relatively soon out of the zone of high baroclinicity, resulting in less intense cyclones at higher latitudes. This could also explain the dipole pattern in EKE shown in Fig. 1b, because in January approximately 50% of all cyclones tracks that propagate through the northern target region also propagate through the southern target region. Thus, to better understand the intensification, in the next section we investigate baroclinic conversion first over the two target regions from an Eulerian viewpoint and afterward along the different tracks ~~from a quasi-Lagrangian viewpoint~~using feature-based cyclone tracking.

6 Baroclinic conversion and its relationship with surface cyclone tracks

6.1 Baroclinic conversion over target regions (Eulerian perspective)

EKE has a baroclinic and barotropic source, and both are known to be affected by midwinter suppression (Schemm and Schneider, 2018). In general, however, the dominant source of EKE is baroclinic conversion. In the following, we first diagnose

[1] A change in SLP larger than 24 hPa within 24 hours normalized to 60°N using $\sin(\phi)/\sin(60°)$ (Sanders and Gyakum, 1980).

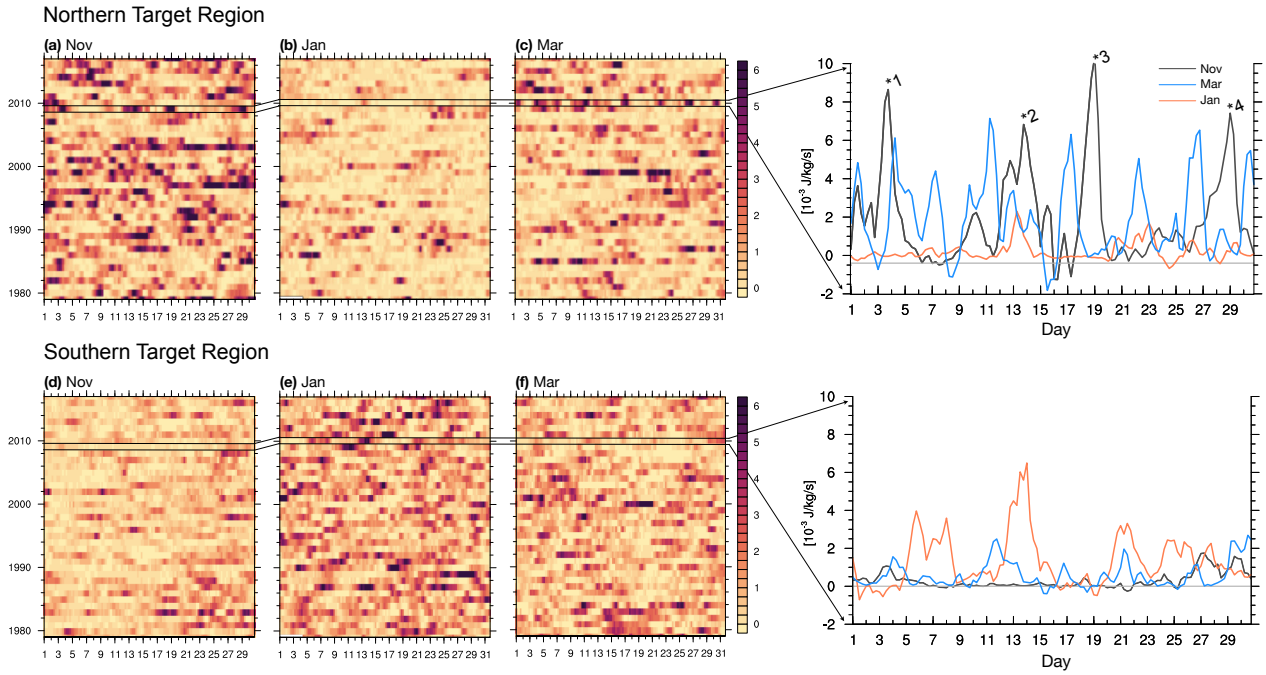

Figure 4. Baroclinic conversion at 500 hPa (10^{-3} J kg^{-1} s^{-1}) averaged over the (a, b, and c) northern and (d, e, and f) southern target regions shown in Fig. 1 for (a and d) November, (b and e) January and (c and f) March for the period 1979–2018. Attached on the right side is a zoomed-in image of the individual time series of daily mean values for November, January, and March 2009/2010.

variations in baroclinic conversions and their link to surface cyclones in the northern and southern target regions on synoptic time scales. The daily mean values of baroclinic conversion, averaged over the northern and southern target regions (see Fig. 1), are shown in Fig. 4 for November, January and March. Baroclinic conversion often peaks at regular intervals of 6-10 days (see the zoom-in for November 2009 and January and March 2010 in the right panels of Fig. 4). These baroclinic conversion bursts result mostly, but not exclusively, from the propagation of deep synoptic systems through the target region. In the northern target region in November 2009 (black contours in the top right panel of Fig. 4), the first and third bursts (labelled "1" and "3" in Fig. 4) are associated with Kuroshio cyclones, while the fourth one is associated with a Kamchatka cyclone that propagates north of the target region but still affects a broader region around it. The second burst (13–15 November) is not associated with a surface cyclone, but with a jet streak development at the edge of an upper-level trough. In November and March (black and blue contours in the top right panel of Fig. 4), the amplitude of the bursts exceeds those in January by a factor of 2–3 (orange contour). The opposite is found in the southern target region, where the baroclinic conversion bursts in January exceed those in November and March. However, the monthly differences in the southern target region are smaller than in the northern target region. Furthermore, the difference between January and March is less clear in the southern target region.

The above findings suggest that the characteristics or the synoptic systems that propagate through the two target regions shown in Fig. 1 clearly differ between the three months. In January, the associated baroclinic conversion is lower than in November and March in the northern target region, and vice versa for the southern region. There are several possible explanations for this behavior, for instance: (i) in midwinter, baroclinic conversion is reduced along the entire life cycle of cyclones in the northern region, or (ii) the life cycles of those cyclone that propagate through both target regions, which are about $\sim 50\%$ of all cyclones that enter the northern target region from the south, have an earlier baroclinic conversion peak (in the southern target region) and reduced baroclinic conversion later in the northern target region. As we show below, the first scenario applies to Kamchatka cyclones and the second one to Kuroshio cyclones. But first, we explore how baroclinic conversion changes during days when a cyclone propagates through the northern target region.

6.2 Baroclinic conversion in the northern target region associated with surface cyclones

In order to quantify the contribution of surface cyclones to the climatological monthly mean baroclinic conversion in the northern region, we split all days into cyclone and non-cyclone days using the surface cyclone tracks. Thereby, we essentially separate deep ~~cyclonic eddies from shallow~~ (tropospheric feeling) eddies, like mature cyclones, and shallow diabatically maintained low-level cyclonic eddies, like diabatic Rossby waves, from upper-level ~~eddies (e.g., shallow~~ eddies, like troughs or ridges~~without surface low- or high-pressure systems) and from deep anticyclonic eddies~~ . Anticyclonic eddies are also excluded. Technically, a surface cyclone track may propagate outside of the northern target region but nevertheless affect the baroclinic conversion inside the target region. We therefore define a cyclone day as a time step when 25 % of the northern target region is covered by a cyclone mask (see section 2 for details). This results in about 50 % cyclone and 50 % non-cyclone days.

Baroclinic conversion is, as expected, larger during cyclone days compared to non-cyclone days (Fig. 5), but baroclinic conversion is not zero during non-cyclone days. Only in January, the median of the baroclinic conversion distribution is near zero for non-cyclone days. The fact that baroclinic conversion is not zero during non-cyclone days can be explained by baroclinic conversion related to an upper-level trough propagating over the northern target region that is not accompanied by a surface cyclone, as is the case for the second burst in Fig. 4 (upper right panel). As clearly shown in Fig. 5, the midwinter suppression affects baroclinic conversion during cyclone and non-cyclone days. Yet, the two distributions differ significantly from each other, in particular in January during midwinter suppression. To test this statistically, we compute 10'000 distributions, each of which consists of randomly selected cyclone and non-cyclone days with replacement. Each randomized distribution is of equal size as there are days in the original cyclone-day distribution. For each randomized distribution, we compute the mean baroclinic conversion, and from the 10'000 mean values the 97.5th and 2.5th percentiles, which are shown as red confidence intervals in Fig. 5. The mean baroclinic conversion values of the cyclone (non-cyclone) day distribution is above (below) the 97.5th (2.5th) confidence intervals in each month. We therefore conclude that the two distributions significantly differ from each other and from a randomized selection. Based on Fig. 5, we conclude that baroclinic conversion in the target region is reduced in midwinter both during cyclone days and non-cyclone days. However, since the baroclinic conversion during cyclone days is higher than during non-cyclone days, the cyclone days contribute ~~much~~ in absolute terms more to the total baroclinic conver-

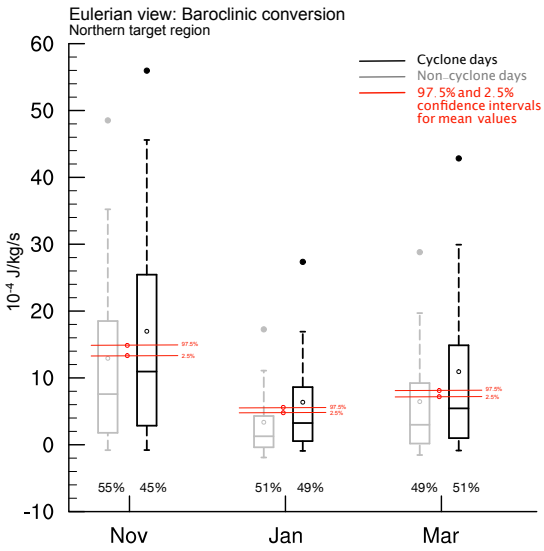

Figure 5. Box-and-whisker diagram for baroclinic conversion at 500 hPa (10^{-4} J kg^{-1} s^{-1}) averaged over the northern target region (gray box in Fig. 1) for days (black) with and (gray) without a surface cyclone affecting the target region (referred to as cyclone and non-cyclone days). Whiskers span between the 10th and 90th percentiles and the box spans the 25th to 75th percentile range. Filled dots indicate the 95th percentile. Open circles indicate the mean value and horizontal lines the median value. The 2.5 and 97.5 confidence intervals of a statistical test (see text for details) are shown in red. Percentage values at the bottom indicate the fraction of days in each sample.

sion in the Pacific storm track~~and accordingly to the reduction in the conversion in midwinter. It is therefore reasonable to focus now only on~~ . Nevertheless, the relative contribution to the suppression is fairly similar. The average baroclinic conversion on a cyclone day reduces from 17 to 6×10^{-4} J kg s^{-1} and on a non-cyclone day from 13 to 3 $\times10^{-4}$J kg s^{-1} and the number of days in each category is close to 50 % (Fig. 5). The separation into cyclone days and ~~the associated tracks~~non-cyclone days is not clear cut. We previously defined non-cyclone days as those days during which the target region is covered by less than 25 % with a cyclone mask. Baroclinic conversion on non-cyclone days thus might still be associated with surface cyclones in close proximity of the target region. In a next step, we investigate ~~the~~ in more details those cyclone tracks that enter the northern target region from the south and compare the baroclinic conversion along these tracks before and after entrance.

6.3 Baroclinic conversion along cyclone tracks outside and inside the northern target region (Lagrangian perspective)

Cyclones that feed the northern target region are Kamchatka cyclones, with genesis inside the target region, and Kuroshio and East China Sea cyclones, which enter the target region from the south. We therefore group all time steps along Kuroshio and East China Sea cyclone tracks into two periods, before and after entering the northern target region. The idea is to see

whether the maximum in baroclinic conversion occurs earlier during the life cycle in January, as suggested in section 5 and based on Tab. 3, and therefore outside the northern target region. In the following, we discuss box-and-whisker diagrams of baroclinic conversion~~and of~~ , the background baroclinicity (Fig. 6 ~~)~~ left) and of the baroclinic conversion efficiency (Fig. 6 right) separately for cyclones that enter the target region from the south (Kuroshio and East China Sea cyclones) for time steps before and after entering the target region, and for Kamchatka cyclones, which reside inside the target region. For all cyclones, baroclinic conversion ~~is~~ and its efficiency are averaged within a 1000 km radius around the cyclone center.

Before entering the northern target region from the south, baroclinic conversion along cyclone tracks is larger in January than in November and March (black boxes in Fig. 6). The distribution of baroclinic conversion outside of the target region exhibits a seasonal cycle that is qualitatively in agreement with the seasonal cycle of the mean baroclinicity equatorward of the target region. The difference between January and March is small, which is a result of the increasing influence of East China Sea cyclone tracks towards late winter and early spring. East China Sea cyclones deepen on average more rapidly than Kuroshio cyclones (Tab. 4) and they are particularly frequent in March (Fig. 2 and Table 1).

After entering the northern target region, baroclinic conversion associated with Kuroshio and East China Sea cyclones is reduced in January compared to November and March, which reflects the midwinter suppression (gray boxes in left panel in Fig. 6). Kuroshio cyclones spend most of their life cycle in the northern target region (percentage of time steps in each category is shown below each box in Fig. 6). In January, the fraction of time steps outside the northern target region is lower than in November and March suggesting that in January cyclones propagate faster poleward and hence out of the zone of high baroclinicity ~~. The strong~~ as original also hypothesized by Nakamura (1992). On their way poleward, the also become less efficient in converting the mean baroclinicity (right panel Fig. 6). The reduction of baroclinic conversion in the northern target region in January occurs despite the fact that the mean baroclinicity along the tracks of Kuroshio cyclones is only marginally reduced compared to other months (horizontal red bars on top of the gray box-and-whiskers in Fig. 6). ~~This confirms the conversion~~ Equatorward of the target region, the baroclinic conversion efficiency in January is higher compared to November, but once Kuroshio cyclones have entered the target region the conversion efficiency reduces and is lower in January. In November, the mean efficiency does even increase when Kuroshio cyclones enter the northen target region. The conversion budget discussed in Schemm and Rivière (2019) ~~, who argued~~ showed that the reduced baroclinic conversion in this region ~~primarily results from a reduction of the eddy conversion efficiency , with only minor contributions form a change in mean baroclinicity~~results indeed from both, a reduction in the mean baroclinicity and conversion efficiency with the conversion efficiency making the larger contribution to the reduction. Overall, the here presented results indicates that Kuroshio cyclones in January deepen rapidly equatorward of the target region and their growth is even strong compared with November and March, but on their way poleward their conversion efficiency decrease (in agreement with the dipole anomaly seen in Fig. 4 in Schemm and Rivière (2019)). The stronger growths in January equatorward of the target region appears to accelerate the life cycle and the cyclones seem to reach earlier during the life cycle a stage when they become less efficient in converting the mean baroclinicity into eddy energy.

In summary, maximum baroclinic conversion along the surface cyclone tracks with genesis over the Kuroshio extension is climatologically largest in January, but occurs equatorward of the northern target region and therefore earlier during the cyclone

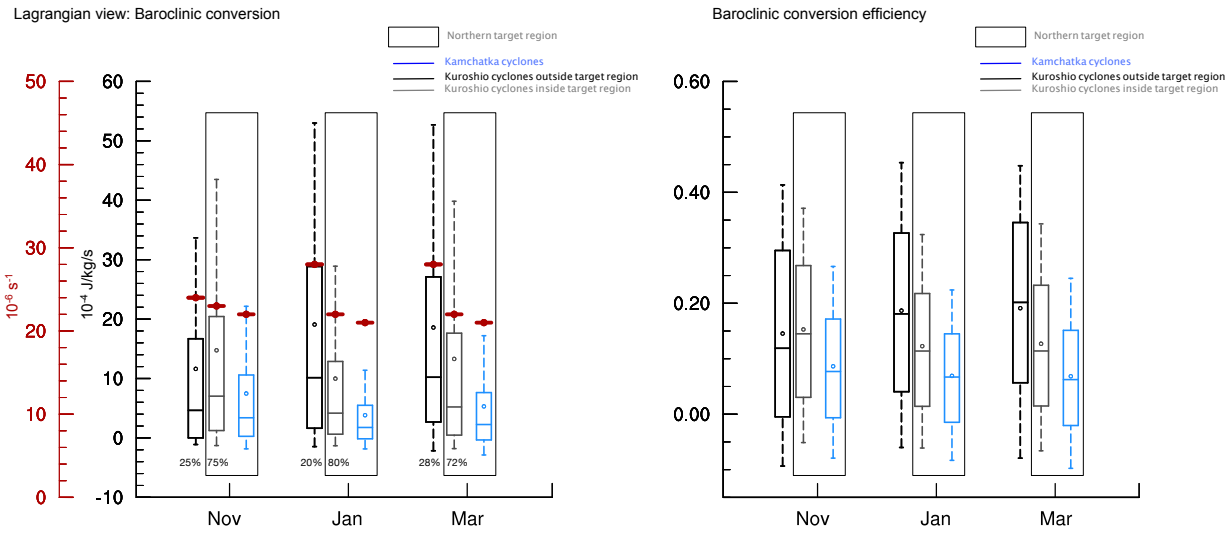

Figure 6. Box-and-whisker diagram for (left) baroclinic conversion at 500 hPa (10^{-4} J kg^{-1} s^{-1}) averaged within a radius of 1000 km around the surface cyclone centers of Kuroshio and East China Sea cyclones, before (black) and after (gray) entering the northern target region, and for Kamchatka cyclones (blue). Additionally shown are the mean background baroclinicity along the tracks (red horizontal lines) and the percentage of time steps before and after entering the target region. (right) Similar as on the left but for the baroclinic conversion efficiency.

life cycle. The larger conversion is thus in agreement with an overall higher mean baroclinicity over the North Pacific, but the equatorward shift of the strengthened baroclinic zone is causing an earlier intensification, because the zone shifts towards the preferred region of Kuroshio cyclogenesis. Kuroshio cyclone not only leave the zone of highest baroclinicity faster in midwinter, but on their way poleward they also become less efficient in converting the mean baroclinicity into eddy energy. For Kamchatka cyclones, baroclinic conversion is reduced in midwinter compared to the shoulder months (blue boxes in Fig. 6), in agreement with the reduced baroclinicity ~~.~~and reduced efficiency (right panel in Fig. 6). The reintensification of Kamchatka cyclones during March occurs despite no notable change in the mean baroclinicity (horizontal red bars on top of the blue box-and-whiskers in Fig. 6), a finding that points again towards ~~the eddy~~ an increase in the baroclinic conversion efficiency as an important moderating process. Kamchatka cyclones contribute with about 40 % to the storm track over the northern target region and their weakening is therefore an important contribution to the suppression.

6.4 Baroclinic conversion along cyclone tracks in a target region that shifts with the maximum in monthly mean baroclinic conversion

In the previous sections, attention was given to baroclinic conversion in a target region that is centered on the location of the maximum reduction in EKE during midwinter. In this section, we explore baroclinic conversion associated with cyclone tracks

that propagate through a target region that shifts with the location of the maximum in monthly mean baroclinic conversion (black target box in Fig. 7). The maximum is located over the western Pacific and shifts equatorward in January. Baroclinic conversion reduces north of approximately 41°N in January and increases south of it (blue shading in Fig. 7a). Next, in line with our previous analysis, we identify all surface cyclone tracks that propagate into this target region from upstream. Fig. 7 show the mean position of the selected tracks (red lines in Fig. 7). The black dots along this mean track indicate the mean location of cyclogenesis, the location of maximum deepening (defined as the largest 6-hourly reduction in mean sea-level pressure), the location of maximum intensity (defined as the minimum in sea-level pressure) and the mean location of cyclolysis. The first result is that the mean location at maximum deepening (second black dot along red line) is in all months either exactly (November, March) or very close to the location of the maximum in monthly mean baroclinic conversion (black contours in Fig. 7). This underlines that the selected tracks play an important role in shaping the monthly mean baroclinic conversion. The mean location of the maximum deepening is located farthest equatorward during January (Fig. 7a). We split these tracks into time steps before and after the cyclones have crossed the latitude of the maximum deepening (dashed line in Fig. 7) and compute box-and-whisker plots of the corresponding baroclinic conversion rates. The results show that in every month, baroclinic conversion rates are higher before the maximum deepening is reached. When comparing the three months, we find that baroclinic conversion is highest during January (black boxes in Fig. 8). The midwinter suppression affects only time steps after maximum deepening (gray boxes in Fig. 8). Consequently, we arrive at similar conclusions. During January, the cyclones benefit from the increased baroclinicity early during the life cycle but due to the equatorward shift of the baroclinic zone the maximum in baroclinic conversion occurs at lower latitudes (second black dot along the red mean track in Fig. 7). However, the cyclones leave the baroclinic zone early on their way poleward, which can be deduced from the mean cyclone tracks in Fig. 7, and baroclinic conversion reduces to levels below that found during November and March after the cyclones crosses the latitude where maximum deepening is observed.

7 Conclusions

This study presents a systematic analysis of the characteristics of cyclone life cycles over the North Pacific, with a particular focus on surface cyclones that propagate through the northwestern Pacific, where EKE decreases during midwinter (referred to as northern target region shown in Fig. 1). The goal of this study is to enrich the existing literature on the midwinter suppression of the North Pacific storm track from a systematic surface cyclone life cycle perspective to understand how cyclone life cycles change ~~in the subtropical jet regime, which typically occurs~~ during midwinter in the western North Pacific.

The surface cyclone tracks feeding the storm track in the northwestern Pacific originate from three preferred regions: (i) downstream of Kamchatka, (ii) over the Kuroshio extension and (iii) over the East China Sea (Fig. 2). Kuroshio and Kamchatka cyclones dominate the total cyclone number over the western North Pacific, while East China Sea cyclones become relevant during spring. Kamchatka and Kuroshio cyclones are preferentially triggered by upper-level waves entering the Pacific through the northern seeding branch, while East China Sea cyclones are at genesis low-level features (Chang, 2005). The analyzed

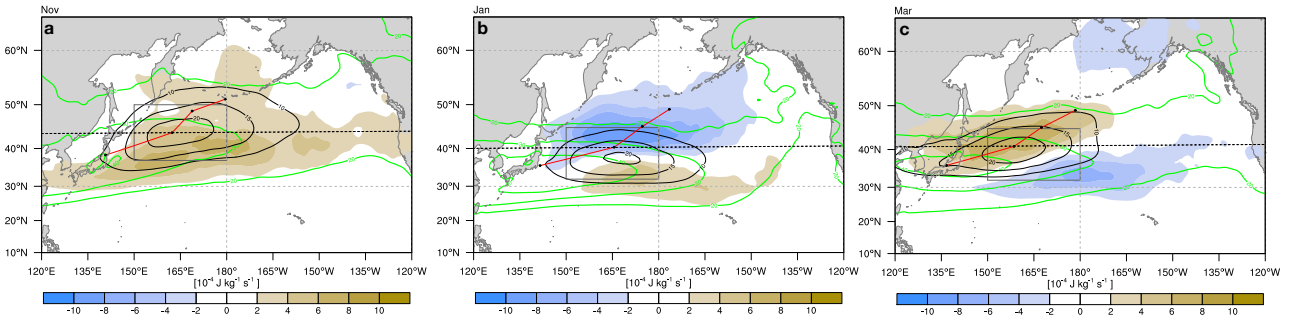

Figure 7. Monthly mean baroclinic conversion at 500 hPa (black contours, 10^{-4} J kg^{-1} s^{-1}) and a target region (black box) that shifts with the maximum in the mean baroclinic conversion for (a) November, (b) January and (c) March. The red line indicates the mean location of cyclone tracks that propagate into the target region from upstream. The black dots along the mean track indicate the mean location of cyclogenesis, the location of maximum deepening (6-hourly SLP change), the location of maximum intensity (minimum SLP) and the location of cyclolysis. Additionally shown are the monthly mean baroclinicity (green contours; 25 to 45 by steps of 5×10^{-6}s^{-1}) and the change of baroclinic conversion relative to the previous months (color shading). The latitude of the maximum deepenng in indicated by a black dashed contour.

tracks have their lysis mostly poleward of their genesis location in the mid-Pacific. The eastern Pacific thus requires further analysis.

Our key findings can be summarized as follows. The equatorward movement of the baroclinic zone in midwinter affects the life cycles of cyclones from all three genesis regions, but in a different way:

- Kamchatka cyclones develop in midwinter in a region of reduced baroclinicity. Compared to November, their lifetime decreases, the time to maximum deepening since genesis reduces and they become less intense. They contribute by about 40 % to the total cyclone number in winter over the northwestern Pacific, where EKE is suppressed. The weakening of Kamchatka cyclones is thus a crucial contribution to the suppression. Interestingly, despite the reduced baroclinicity in January, the number of Kamchatka cyclones is not reduced in midwinter. Kamchatka cyclones do not re-intensify during March, thus they do not benefit from the poleward movement of the baroclinic zone in spring.

- East China Sea, benefit from the equatorward movement of the baroclinic zone in midwinter. Compared to November, they become more intense, the fraction of explosively deepening cyclones increases and their lifetime extends. They become weaker in March, but the fraction of explosively deepening life cycles remains higher than for Kuroshio and Kamchatka cyclones. In addition, their lifetime is longer in March compared to January. In March, East China Sea cyclones contribute by nearly 22% to the total cyclone number over the northwestern Pacific, while in fall and winter their contribution is approximately 15%. Thus, they seem to play a role in the re-intensification of the storm track during spring.

– The changes in the life cycles of Kuroshio cyclones are the most complex, but understanding these changes is crucial, because Kuroshio cyclones contribute strongest to the total cyclone number in the northern target region in midwinter (45%). Compared to the shoulder months, in January the lifetime of Kuroshio cyclones and the time to maximum deepening are shortest. The fraction of ~~explosively deepening cyclones~~ cyclones satisfying the "bomb cyclogenesis" criterion (Sanders and Gyakum, 1980) first reduces from November to January but then remains at similar levels until March. ~~Highest values in baroclinic conversion are found during midwinter~~However, highest values in 6-hourly baroclinic conversion rates are found in January, but these occur at lower latitudes ~~, south of the northern target region,~~ and they are sustained for a reduced number of time steps relative to the shoulder months. In terms of minimum sea level pressure, Kuroshio cyclones are however most intense in January.

Overall, it seems as if during midwinter the life cycle of a Kuroshio cyclone is best characterized by a short and intense early deepening, in agreement with the higher baroclinicity, followed by a fast decay and poleward propagation away from the more equatorward located baroclinic zone. According to this interpretation, we observe an acceleration of the Kuroshio life cycle during midwinter. This interpretation is in agreement with the idea of a reduced baroclinic conversion efficiency because the efficiency is dictated by the vertical tilt of a cyclone (Schemm and Rivière, 2019). Acceleration of the life cycle with intense early growth results in cyclones that acquire a rather inefficient vertical tilt earlier in the life cycle. Kuroshio cyclones are thus in different months in different stages of their life cycle at similar latitudes. The stronger but earlier deepening followed by an earlier decay is the ~~quasi-Lagrangian~~ cyclone life-cycle perspective on the ~~equatorward shift seen in EKE from an Eulerian perspective (Fig. 1b).~~ midwinter suppression over the western Pacific.

7.1 Caveats

Our results are based on a single object-based cyclone detection scheme. It is known that cyclone tracks are sensitive to the identification and tracking scheme Neu et al. (2013), this holds also true for the genesis location. While they typically agree on deep systems, a higher sensitive must be expected for shallow systems, as is the case for Kamchatka cyclones in January. Further, we ignore short-lived systems with a lifetime of less than 24 hours. Such systems might become more frequent in midwinter because the lifetime of all systems is reduced in January. Baroclinic conversion occurs also in the absence of surface cyclones, for example by the propagation of an upper-level trough, like the second baroclinic conversion peak in Fig. 4. Baroclinic conversion during non-cyclone days is also affected by the midwinter suppression and this reduction is not explained by our study. Our study has its focus on the western North Pacific, where climatological mean baroclinicity is highest and the reduction in baroclinic conversion and EKE is thus most surprising. Cyclone tracks that feed the eastern North Pacific are generated over the central-east Pacific (Hoskins and Hodges, 2002; Wernli and Schwierz, 2006) where climatologically baroclinicy is much lower compared with the western Pacific. Cyclone tracks over the eastern North Pacific not surprisingly have a large fraction of secondary cyclones (Fig. 5b in Schemm et al., 2018). Mechanisms responsible for the suppression in the eastern North Pacific thus require further analysis.

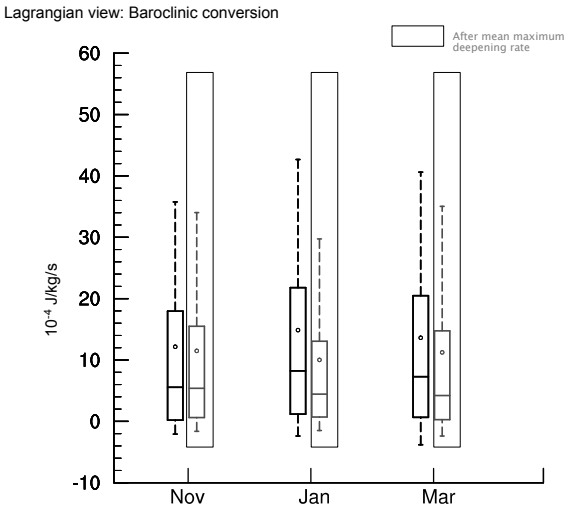

Figure 8. Box-and-whisker diagram for baroclinic conversion at 500 hPa (10^{-4} J kg^{-1} s^{-1}) averaged within a radius of 1000 km around the surface cyclone centers that enter the target region in Fig. 7 from upstream, before (black) and after (gray) passing the latitude of maximum deepening (black dashed line in Fig. 7).

Author contributions. All three authors contributed to the discussion and final interpretation of the results. HB and SeS performed the analyses. SeS wrote, supported by HB and HW, the publication.

Competing interests. The authors declare no competing interests.

Acknowledgements. The authors acknowledge the discussions on the midwinter suppression with various colleagues at the 2018 storm track workshop on Utö, Sweden. SeS has received funding from the European Research Council (ERC) under the European Union's Horizon 2020 research and innovation programme (grant agreement No. 848698). HB acknowledges funding from the Swiss National Science Foundation (SNSF) via grants 146834 and 185049. We thank MeteoSwiss and ECMWF for access to the ERA-Interim reanalyses.

References

Afargan, H. and Kaspi, Y.: A Midwinter Minimum in North Atlantic Storm Track Intensity in Years of a Strong Jet, Geophys. Res. Lett., 44, 12,511–12,518, https://doi.org/10.1002/2017GL075136, 2017.

Boettcher, M. and Wernli, H.: A 10-yr Climatology of diabatic Rossby waves in the Northern Hemisphere, Mon. Wea. Rev., 141, 1139–1154, https://doi.org/10.1175/MWR-D-12-00012.1, 2013.

Chang, E. K. M.: GCM and Observational Diagnoses of the Seasonal and Interannual Variations of the Pacific Storm Track during the Cool Season, J. Atmos. Sci., 58, 1784–1800, https://doi.org/10.1175/1520-0469(2001)058<1784:GAODOT>2.0.CO;2, 2001.

Chang, E. K. M.: The Impact of Wave Packets Propagating across Asia on Pacific Cyclone Development, Mon. Wea. Rev., 133, 1998–2015, https://doi.org/10.1175/MWR2953.1, 2005.

Chang, E. K. M. and Guo, Y.: Comments on The Source of the Midwinter Suppression in Storminess over the North Pacific, J. Climate, 24, 5187–5191, https://doi.org/10.1175/2011JCLI3987.1, 2011.

Chang, E. K. M. and Guo, Y.: Is Pacific Storm-Track Activity Correlated with the Strength of Upstream Wave Seeding?, J. Climate, 25, 5768–5776, https://doi.org/10.1175/JCLI-D-11-00555.1, 2012.

Deng, Y. and Mak, M.: An idealized model study relevant to the dynamics of the midwinter minimum of the Pacific storm track, J. Atmos. Sci., 62, 1209–1225, https://doi.org/10.1175/JAS3400.1, 2005.

Gilet, J.-B., Plu, M., and Rivière, G.: Nonlinear Baroclinic Dynamics of Surface Cyclones Crossing a Zonal Jet, J. Atmos. Sci., 66, 3021–3041, https://doi.org/10.1175/2009JAS3086.1, https://doi.org/10.1175/2009JAS3086.1, 2009.

Harnik, N. and Chang, E. K. M.: The Effects of Variations in Jet Width on the Growth of Baroclinic Waves: Implications for Midwinter Pacific Storm Track Variability, J. Atmos. Sci., 61, 23–40, https://doi.org/10.1175/1520-0469(2004)061<0023:TEOVIJ>2.0.CO;2, 2004.

Hoskins, B. J. and Hodges, K. I.: New Perspectives on the Northern Hemisphere Winter Storm Tracks, Journal of the Atmospheric Sciences, 59, 1041–1061, https://doi.org/10.1175/1520-0469(2002)059<1041:NPOTNH>2.0.CO;2, 2002.

Hoskins, B. J., McIntyre, M. E., and Robertson, A. W.: On the use and significance of isentropic potential vorticity maps, Quart. J. Roy. Meteor. Soc., 111, 877–946, 1985.

James, I. N.: Suppression of Baroclinic Instability in Horizontally Sheared Flows, J. Atmos. Sci., 44, 3710–3720, https://doi.org/10.1175/1520-0469(1987)044<3710:SOBIIH>2.0.CO;2, 1987.

Lindzen, R. S. and Farrell, B.: A Simple Approximate Result for the Maximum Growth Rate of Baroclinic Instabilities, J. Atmos. Sci., 37, 1648–1654, https://doi.org/10.1175/1520-0469(1980)037<1648:ASARFT>2.0.CO;2, 1980.

Lorenz, E. N.: Available Potential Energy and the Maintenance of the General Circulation, Tellus, 7, 157–167, https://doi.org/10.3402/tellusa.v7i2.8796, 1955.

Nakamura, H.: Midwinter Suppression of Baroclinic Wave Activity in the Pacific, J. Atmos. Sci., 49, 1629–1642, https://doi.org/10.1175/1520-0469(1992)049<1629:MSOBWA>2.0.CO;2, 1992.

Nakamura, H. and Sampe, T.: Trapping of synoptic-scale disturbances into the North-Pacific subtropical jet core in midwinter, Geophys. Res. Lett., 29, 8–1–8–4, https://doi.org/10.1029/2002GL015535, 2002.

Nakamura, N.: An Illustrative Model of Instabilities in Meridionally and Vertically Sheared Flows, J. Atmos. Sci., 50, 357–376, https://doi.org/10.1175/1520-0469(1993)050<0357:AIMOII>2.0.CO;2, 1993.

Neu, U., Akperov, M. G., Bellenbaum, N., Benestad, R., Blender, R., Caballero, R., Cocozza, A., Dacre, H. F., Feng, Y., Fraedrich, K., Grieger, J., Gulev, S., Hanley, J., Hewson, T., Inatsu, M., Keay, K., Kew, S. F., Kindem, I., Leckebusch, G. C., Liberato, M. L. R., Lionello,

P., Mokhov, I. I., Pinto, J. G., Raible, C. C., Reale, M., Rudeva, I., Schuster, M., Simmonds, I., Sinclair, M., Sprenger, M., Tilinina, N. D., Trigo, I. F., Ulbrich, S., Ulbrich, U., Wang, X. L., and Wernli, H.: IMILAST: A Community Effort to Intercompare Extratropical Cyclone Detection and Tracking Algorithms, Bull. Amer. Meteor. Soc., 94, 529–547, https://doi.org/10.1175/BAMS-D-11-00154.1, 2013.

Novak, L., Schneider, T., and Ait-Chaalal, F.: Midwinter Suppression of Storm Tracks in an Idealized Zonally Symmetric Setting, J. Atmos. Sci., 77, 297–313, https://doi.org/10.1175/JAS-D-18-0353.1, 2020.

Orlanski, I. and Katzfey, J.: The Life Cycle of a Cyclone Wave in the Southern Hemisphere. Part I: Eddy Energy Budget, J. Atmos. Sci., 48, 1972–1998, https://doi.org/10.1175/1520-0469(1991)048<1972:TLCOAC>2.0.CO;2, 1991.

Oruba, L., Lapeyre, G., and Rivière, G.: On the Poleward Motion of Midlatitude Cyclones in a Baroclinic Meandering Jet, Journal of the Atmospheric Sciences, 70, 2629–2649, https://doi.org/10.1175/JAS-D-12-0341.1, https://doi.org/10.1175/JAS-D-12-0341.1, 2013.

Park, H.-S., Chiang, J. C. H., and Son, S.-W.: The Role of the Central Asian Mountains on the Midwinter Suppression of North Pacific Storminess, J. Atmos. Sci., 67, 3706–3720, https://doi.org/10.1175/2010JAS3349.1, 2010.

Penny, S., Roe, G. H., and Battisti, D. S.: The Source of the Midwinter Suppression in Storminess over the North Pacific, J. Climate, 23, 634–648, https://doi.org/10.1175/2009JCLI2904.1, 2010.

Penny, S. M., Roe, G. H., and Battisti, D. S.: Reply, J. Climate, 24, 5192–5194, https://doi.org/10.1175/2011JCLI4187.1, 2011.

Penny, S. M., Battisti, D. S., and Roe, G. H.: Examining Mechanisms of Variability within the Pacific Storm Track: Upstream Seeding and Jet-Core Strength, J. Climate, 26, 5242–5259, https://doi.org/10.1175/JCLI-D-12-00017.1, 2013.

Rivière, G., Arbogast, P., Lapeyre, G., and Maynard, K.: A potential vorticity perspective on the motion of a mid-latitude winter storm, Geophysical Research Letters, 39, https://doi.org/10.1029/2012GL052440, 2012.

Rivière, G., Berthou, S., Lapeyre, G., and Kageyama, M.: On the Reduced North Atlantic Storminess during the Last Glacial Period: The Role of Topography in Shaping Synoptic Eddies, J. Climate, 31, 1637–1652, https://doi.org/10.1175/JCLI-D-17-0247.1, 2018.

Sanders, F. and Gyakum, J. R.: Synoptic-dynamic climatology of the "bomb", Mon. Wea. Rev., 108, 1589–1606, https://doi.org/10.1175/1520-0493(1980)108<1589:SDCOT>2.0.CO;2, 1980.

Schemm, S. and Rivière, G.: On the Efficiency of Baroclinic Eddy Growth and How It Reduces the North Pacific Storm-Track Intensity in Midwinter, J. Climate, 32, 8373–8398, https://doi.org/10.1175/JCLI-D-19-0115.1, 2019.

Schemm, S. and Schneider, T.: Eddy Lifetime, Number, and Diffusivity and the Suppression of Eddy Kinetic Energy in Midwinter, J. Climate, 31, 5649–5665, https://doi.org/10.1175/JCLI-D-17-0644.1, 2018.

Schemm, S., Sprenger, M., and Wernli, H.: When during Their Life Cycle Are Extratropical Cyclones Attended by Fronts?, Bulletin of the American Meteorological Society, 99, 149–165, https://doi.org/10.1175/BAMS-D-16-0261.1, https://doi.org/10.1175/BAMS-D-16-0261.1, 2018.

Sprenger, M., Fragkoulidis, G., Binder, H., Croci-Maspoli, M., Graf, P., Grams, C. M., Knippertz, P., Madonna, E., Schemm, S., Škerlak, B., et al.: Global climatologies of Eulerian and Lagrangian flow features based on ERA-Interim, Bull. Amer. Meteor. Soc., 98, 1739–1748, 2017.

Wernli, H. and Schwierz, C.: Surface Cyclones in the ERA-40 Dataset (1958–2001). Part I: Novel Identification Method and Global Climatology, J. Atmos. Sci., 63, 2486–2507, https://doi.org/10.1175/JAS3766.1, 2006.

Yuval, J., Afargan, H., and Kaspi, Y.: The Relation Between the Seasonal Changes in Jet Characteristics and the Pacific Midwinter Minimum in Eddy Activity, Geophys. Res. Lett., 45, 9995–10 002, https://doi.org/10.1029/2018GL078678, 2018.

Mean EKE at the 500 hPa level (black contours at 85, 95, and 105 J kg^{-1}) and corresponding change relative to the corresponding previous month (color shading) for (a) November, (b) January and (c) March. Additionally shown are two target regions (gray boxes) that are used for the detailed diagnostics of surface cyclone tracks throughout this study.

Cyclogenesis frequency (color shading; %) for surface cyclone tracks that propagate through the northern (left column) and southern (right column) target regions (shown as a gray box) for (a,b) November, (c,d) January and (e,f) March. Additionally shown are EKE (black contours; 85, 95, and 105 J kg^{-1}) and baroclinicity (green contours; 25 to 45 by steps of 5$\times$10^{-6}s^{-1}) at the 500-hPa level

Relative contributions (color shading; %) of (a, c and e) Kamchatka cyclones and (b, d and f) Kuroshio combined with East China Sea cyclones to the total surface cyclone frequency in the northern target region (gray box). The contours show the change in EKE relative to the corresponding previous month (solid lines are for positive values, and dashed lines for negative values; -20 to 20 J kg^{-1} by steps of 5 J kg^{-1}).

Baroclinic conversion at 500 hPa (10^{-3} J kg^{-1} s^{-1}) averaged over the (a, b, and c) northern and (d, e, and f) southern target regions shown in Fig. 1 for (a and d) November, (b and e) January and (c and f) March for the period 1979–2018. Attached on the right side is a zoomed-in image of the individual time series of daily mean values for November, January, and March 2009/2010.

Box-and-whisker diagram for baroclinic conversion at 500 hPa (10^{-4} J kg^{-1} s^{-1}) averaged over the northern target region (gray box in Fig. 1) for days (black) with and (gray) without a surface cyclone affecting the target region (referred to as cyclone and non-cyclone days). Whiskers span between the 10th and 90th percentiles and the box spans the 25th to 75th percentile range. Filled dots indicate the 95th percentile. Open circles indicate the mean value and horizontal lines the median value. The 2.5 and 97.5 confidence intervals of a statistical test (see text for details) are shown in red. Percentage values at the bottom indicate the fraction of days in each sample.

Box-and-whisker diagram for baroclinic conversion at 500 hPa (10^{-4} J kg^{-1} s^{-1}) averaged within a radius of 1000 km around the surface cyclone centers of Kuroshio and East China Sea cyclones, before (black) and after (gray) entering the northern target region, and for Kamchatka cyclones (blue). Additionally shown are the mean background baroclinicity along the tracks (red horizontal lines) and the percentage of time steps before and after entering the target region.

(First column) Total number of surface cyclones in the northern target region and number of cyclones per day in parenthesis (1980–2018). (Second column) Fraction and number (in parenthesis) of Kamchatka, (third column) Kuroshio and (fourth column) East China Sea cyclones. The northern target region is shown in Fig. 1.Cyclones in target region Kamchatka Kuroshio East China Sea November 507 [0.43] 45 % [229] 41 % [207] 14 % [71] January 516 [0.43] 40 % [206] 46 % [236] 14 % 74March 527 [0.44] 39 % 20839 % [204] 22 % [115]

Lifetime (hours) of surface cyclones passing through the northern target region according to their genesis regions.Kamchatka Kuroshio East China Sea November 77 98 117 January 62 86 132 March 70 91 172

Time to maximum deepening since genesis (hours) of surface cyclones passing through the northern target region according to their genesis regions.Time to maximum deepeningKamchatka Kuroshio East China Sea November 35 29 43 January 26 21 39 March 31 23 42

~~Minimum sea level pressure of surface cyclones passing through the northern target region according to genesis regions and, in parenthesis, the fraction of cyclones satisfying the criterion for "bomb cyclogenesis" (deepening larger than 24 hPa within 24 hours normalized to 60°N.)Minimum SLP (hPa) and fraction of "cyclone bombs" Kamchatka Kuroshio East China Sea November 979.4 21 %975.8 49 %975.7 63 %January 982.9 7 %973.6 42 %967.2 76 %March 987.3 7 %979.0 43 %971.4 65 %~~